

# Important Notice

This copy may be used only for the purposes of research and private study, and any use of the copy for a purpose other than research or private study may require the authorization of the copyright owner of the work in question. Responsibility regarding questions of copyright that may arise in the use of this copy is assumed by the recipient.

UNIVERSITY OF CALGARY

Integrated geological and geophysical analysis of  
a heavy-oil reservoir at Pikes Peak, Saskatchewan

by

Ian Andrew Watson

A THESIS

SUBMITTED TO THE FACULTY OF GRADUATE STUDIES  
IN PARTIAL FULFILMENT OF THE REQUIREMENTS FOR THE  
DEGREE OF MASTER OF SCIENCE

DEPARTMENT OF GEOLOGY AND GEOPHYSICS

CALGARY, ALBERTA

JANUARY, 2004

© Ian Andrew Watson 2004

UNIVERSITY OF CALGARY  
FACULTY OF GRADUATE STUDIES

The undersigned certify that they have read, and recommended to the Faculty of Graduate Studies for acceptance, a thesis entitled: “Integrated geological and geophysical analysis of a heavy-oil reservoir at Pikes Peak, Saskatchewan” submitted by Ian Andrew Watson in partial fulfillment of the requirements for the degree of Master of Science.

---

Supervisor, Dr. Laurence R. Lines, Department of Geology and Geophysics

---

Dr. Robert R. Stewart, Department of Geology and Geophysics

---

Dr. S. A. (Raj) Mehta, Department of Chemical and Petroleum Engineering

---

Date

## Abstract

Various seismic techniques can be used for monitoring zones of steam injection in heavy-oil recovery. In this integrated case study, post-stack interpretation based analysis techniques are used to delineate steamed and heated reservoir zones at Husky Energy's Pikes Peak heavy-oil field in Saskatchewan. Four methods are compared including reflectivity differencing, impedance differencing, P-wave traveltimes ratios, and an isochron method for examining  $V_p/V_s$ . All methods show promise and consistency for delineating areas of steam injection and temperature increase in the reservoir away from well control.

The integration of well and seismic data reveals methods to further understand the reservoir. The percentage of sand in the reservoir interval is estimated using  $V_p/V_s$ . The reservoir trap and bottom-water presence are interpreted using isochron measurements of a deeper interval.

A single multicomponent seismic survey is a powerful tool for reservoir surveillance and interpretation at any stage of field development.

## **Acknowledgements**

Dr. Larry Lines, my thesis supervisor, has provided constant encouragement and demonstrated great patience. I thank my employer, Imperial Oil Resources, for permission to take an education leave of absence and co-sponsoring an NSERC Industrial Scholarship. Husky Energy Ltd. provided the seismic and well data. The March 2000 seismic data acquisition was done by Veritas DGC Land. The seismic data were processed by Matrix Geoservices Ltd. Core measurements were made by Core Laboratories Ltd. Software and user support were provided by GeoGraphix (Landmark Graphics Corporation), Fugro-Jason Canada (Jason Geosystems) and Hampson-Russell. IHS Accumap was used to access well data and digital well logs. AOSTRA (Alberta Oil Sands Technology Research Authority) and COURSE (Core University Research in Sustainable Energy) provided funding for the heavy-oil research group in the Department of Geology and Geophysics.

I acknowledge CREWES (Consortium for Research in Elastic Wave Exploration Seismology) sponsors, staff and students for funding, computers, software and all kinds of help. I give special thanks to Katherine Brittle, Ayon Dey, Brian Hoffe, Mark Kirtland, Henry Bland and Kevin Hall for their individual contributions.

I thank family and friends for their ongoing support and encouragement.

Most of all, I thank Shari, my wife, for her sacrifice of time and love.

## **Dedication**

To Shari

# Table of Contents

<b>Abstract</b> .....	<b>iii</b>
<b>Acknowledgements</b> .....	<b>iv</b>
<b>Dedication</b> .....	<b>v</b>
<b>Table of Contents</b> .....	<b>vi</b>
<b>List of Tables</b> .....	<b>viii</b>
<b>List of Figures</b> .....	<b>ix</b>
<b>Glossary of Terms</b> .....	<b>xi</b>
<b>Chapter 1 Introduction and Background</b> .....	<b>1</b>
1.1 Heavy-oil recovery.....	1
1.2 Previous related work .....	4
1.3 The Pikes Peak Field.....	6
1.3.1 Location .....	6
1.3.2 Field History .....	7
1.3.3 Reservoir Parameters .....	12
1.4 Data.....	12
1.4.1 Geological data .....	13
1.4.2 Geophysical data.....	15
1.4.3 Engineering data .....	19
1.5 Software and Hardware.....	20
<b>Chapter 2 Reservoir Characterization</b> .....	<b>21</b>
2.1 Stratigraphy.....	21
2.1.1 Homogenous Sand Unit.....	27
2.1.2 Interbedded Sand and Shale Unit.....	28
2.1.3 Shale Unit .....	29
2.2 Structure.....	30
2.3 Core analysis.....	37
2.4 Temperature Data.....	40
<b>Chapter 3 Impedance Inversion</b> .....	<b>42</b>
3.1 Inversion Theory .....	42
3.2 Inversion Process Overview .....	44
3.2.1 Synthetic Tie and Interpretation.....	46
3.2.2 Earth Model .....	48
3.2.3 Inversion .....	48
3.2.4 Trace Merge.....	50
<b>Chapter 4 Time-lapse Analysis</b> .....	<b>53</b>
4.1 Introduction.....	53
4.2 Reflectivity Differencing .....	56
4.3 Impedance Section Differencing.....	58
4.4 Isochron analysis.....	59

<b>Chapter 5 Multicomponent Analysis .....</b>	<b>62</b>
5.1 Introduction.....	62
5.2 $V_p/V_s$ Interpretation .....	66
5.3 $V_p/V_s$ Steam Front Analysis .....	69
5.4 $V_p/V_s$ Sand Percent Analysis.....	71
<b>Chapter 6 Conclusions.....</b>	<b>75</b>
6.1 Conclusions.....	75
6.2 Future Research .....	78
<b>References.....</b>	<b>80</b>
<b>Appendix A General Well Data.....</b>	<b>84</b>
<b>Appendix B Matrix Seismic Processing Flows .....</b>	<b>85</b>
H1991.....	85
H2000 Geophone Array.....	86
H2000 Vertical Component .....	87
H2000 Radial Component.....	88
<b>Appendix C Engineering Well Data.....</b>	<b>89</b>

## List of Tables

Table 1-1: Summary of Waseca reservoir parameters at Pikes Peak.....	12
Table 1-2: Summary of 2D survey differences at Pikes Peak. ....	16
Table 2-1: Comparison of core analysis at reservoir condition before and after steam-flood. ....	39
Table 4-1: Predicted steam zone radii and time (in months) since steam was injected into key wells adjacent to H1991 and H2000. ....	55
Table 6-1: Summary of seismic interpretation and analysis techniques at Pikes Peak. ...	76
Table A-1: Summary of 24 Pikes Peak wells adjacent to H1991 and H2000 seismic lines. ....	84
Table C-1: Husky engineering data as of February 15, 1991 .....	89
Table C-2: Husky engineering data as of March 1, 2000 .....	90

## List of Figures

Figure 1-1: Map of major heavy-oil deposits of Alberta and Saskatchewan.....	7
Figure 1-2: Production history from the Pikes Peak Waseca Formation.....	8
Figure 1-3: (a) Map view of inverted 7-spot honeycomb pattern and (b) Conceptual 3D view. ....	9
Figure 1-4: Map of the Pikes Peak Field. ....	13
Figure 1-5: Typical log suite used for well log interpretation over the zone of interest...	14
Figure 1-6: H1991 reflectivity section.....	18
Figure 1-7: H2000 (vertical array) reflectivity section. ....	18
Figure 2-1: Generalized Stratigraphic Chart for the Pikes Peak area. ....	21
Figure 2-2: Waseca incised valley trend in the Pikes Peak area.....	23
Figure 2-3: Waseca incised valley facies at Pikes Peak. ....	24
Figure 2-4: West-east structural cross section through Pikes Peak .....	24
Figure 2-5: Map of the east side of the Pikes Peak field .....	25
Figure 2-6: Structural cross-section A-A' constructed using gamma ray logs .....	26
Figure 2-7: Map of the greater Lloydminster area.....	31
Figure 2-8: Structural cross-section B-B' created with sonic logs. ....	31
Figure 2-9: Synthetic tie from well 10-09 to H2000 over the Devonian section.....	33
Figure 2-10: H2000 seismic line with an interpretation of the top and base of the Prairie Evaporite .....	34
Figure 2-11: Chart of the time thickness of the Prairie Evaporite and the structural position of bottom water.....	34
Figure 2-12: Gamma ray and resistivity logs from sample well, 1A15-6 .....	35
Figure 2-13: Effect of temperature on $V_P$ and $V_S$ from core samples. ....	38
Figure 2-14: 6A2-6 temperature log over the Waseca interval.....	41
Figure 3-1: Simple two layer impedance model.....	42
Figure 3-2: Composition of a sonic log .....	44
Figure 3-3: Summary of the H2000 inversion process .....	45
Figure 3-4: Interpreted (a) H1991 and (b) H2000 .....	47

Figure 3-5: Constraint editor for CSSI.....	49
Figure 3-6: Trace merge filter design .....	51
Figure 3-7: Full acoustic impedance section of H1991 .....	52
Figure 3-8: Full acoustic impedance section of H1991 .....	52
Figure 4-1: Maps of the Pikes Peak field in (a) February 1991 and (b) March 2000.....	53
Figure 4-2: Schematic to illustrate how the steam zone projects on to the 2D seismic lines. ....	56
Figure 4-3: Seismic reflectivity difference section.....	57
Figure 4-4: Acoustic impedance difference section.....	58
Figure 4-5: H2000/H1991 ratio of Waseca interval traveltimes for P-wave arrivals. ....	60
Figure 5-1: Traveltimes through a constant thickness interval for compressional and converted waves. ....	62
Figure 5-2: P- and S- wave velocity logs from the dipole sonic log at well 1A15-6.....	65
Figure 5-3: Converted P-S-wave synthetic created at 1A15-6. ....	67
Figure 5-4: Interpreted H2000 P-P section (vertical component).....	68
Figure 5-5: Interpreted H2000 P-S section (radial component).....	68
Figure 5-6: $V_p/V_s$ plot of Waseca-Sparky interval.....	69
Figure 5-7: $V_p/V_s$ plot of Mannville-Lower Mannville interval. ....	70
Figure 5-8: Comparison of $V_p/V_s$ trend line with percent sand .....	72
Figure 5-9: Gamma ray log from well 3B9-6 indicating 57 percent sand .....	72
Figure 5-10: Cross plot of $V_p/V_s$ trend line versus percent Waseca sand .....	73

## Glossary of Terms

This glossary of technical terms provides context and meaning to many expressions and words used in this thesis (after Bates and Jackson, 1984, Sheriff, 1991, Meyer and De Witt Jr., 1990, and Miller, 1996).

**3-C seismic survey:** A three-component (3-C) seismic survey which uses a conventional energy source and is recorded with geophones that respond to ground motions in three orthogonal directions.

**Acoustic Impedance:** A rock property which is defined as the product of rock density and P-wave velocity.

**API Gravity:** A standard adopted by the American Petroleum Institute for expressing the specific weight of oils. ( $^{\circ}\text{API gravity} = 141.5/\text{specific gravity at } 60^{\circ}\text{F} - 131.5$ )

**API Units:** A unit of counting rate for the gamma-ray log. The difference between the high and low radioactivity sections in the American Petroleum Institute calibration pit is defined as 200 API units.

**Bandpass filter:** A filter which allows the passage of a specified frequency range and attenuates others.

**Bitumen:** Natural bitumen shares attributes of heavy oil but is more viscous (greater than 10 000 mPa.s) and more dense. Bitumen is also known as tar sands or oil sands.

**CDP:** Common depth point representing the midpoint between a source and receiver.

**Dipole sonic log:** Sonic logging tool with dipole source that records P- and S-wave transit times.

**Earth model:** In this thesis, a 2D geologic model of the subsurface defined by geological boundaries and populated with rock properties.

**Evaporite:** Sediment that is deposited from aqueous solution as a result of extensive or total evaporation (e.g. rock salt).

**Fresnel Zone:** An area that defines the lateral spatial resolution of seismic data. The resolution decreases with increasing depth.

**Interbedded:** Strata or beds that lie between or alternate with others of different character or composition. In this thesis, the alternating beds are sand and shale.

**Isochron:** In this thesis, the time thickness or interval travelttime between two interpreted seismic horizons.

**Heavy oil:** A type of crude petroleum characterized by high viscosity (less than 10 000 mPa.s), and API gravity between 10 and 20° API. The crude oil at Pikes Peak is commonly called heavy oil.

**Mode:** Refers to the type of wave propagation (P-wave or S-wave).

**Multicomponent seismic:** Seismic data acquired with more than one source and/or receiver mode.

**P-wave:** An elastic body (pressure) wave in which particle motion is in the direction of propagation.

**P-P seismic:** P-waves travelling down to a surface and reflecting back as a P-wave. In this thesis, particle motion recorded on a vertical geophone are assumed to be largely P-P mode.

**P-S seismic:** P-waves travelling down to a surface and reflecting back as an S-wave. In this thesis, particle motion recorded on a radial geophone are assumed to be largely P-S mode.

**Radial component:** Horizontal geophone coil which responds to horizontal ground motion in line with the source-receiver azimuth.

**Siderite:** An iron carbonate mineral that forms in the pore space of clastic rocks and occludes porosity.

**Static:** Time correction applied to seismic data to compensate for the effects of variations in elevation, weathering thickness, weathering velocity, or reference to a datum.

**Steam-oil ratio (SOR):** The relative amount of steam injected into a reservoir to the amount of oil produced.

**S-wave:** An elastic body (shear) wave in which particle motion is perpendicular to the direction of propagation.

**Synthetic seismogram:** An artificial seismic record formed by convolving a wavelet with a reflectivity series.

**Transverse component:** Horizontal geophone coil which responds to horizontal ground motion orthogonal to the source-receiver azimuth.

**Vertical component:** Vertical geophone coil which responds to vertical ground motion.

**Vibroseis:** A seismic method in which a vibrator is used as an energy source. The vibrator generates waves of continuously varying frequency content.

**Viscosity:** Resistance of a fluid to flow.

**$V_P$ :** P-wave velocity.

**$V_P/V_S$ :** Ratio of P-wave velocity to S-wave velocity.

**$V_S$ :** S-wave velocity.

## Chapter 1

### Introduction and Background

#### 1.1 Heavy-oil recovery

With the decline of conventional oil production in the Western Canadian Basin, the profile of heavy-oil is raised. Billions of dollars have been invested in the oil sands regions in the past decade as companies position themselves for future production volumes. The risk of resource presence is small but the methods for extracting the heavy oil are complex and capital intensive. The difficulty in production arises because of the extremely high viscosity of oil sands.

In the Ft. McMurray area of Alberta, where the heavy-oil or bitumen resource is at the surface or very shallow, mining operations are employed. In areas where the overburden is too thick for mining other methods of extraction are required. Usually this involves the use of steam. Two methods have been commercially employed – active and passive. The active method involves the use of high-pressure steam to penetrate and heat the reservoir rock formation and reduce the viscosity of the oil. The oil is produced from either the same wellbore or closely spaced neighbouring wellbores. Imperial Oil's Cold Lake, Alberta field and Husky Energy's Pikes Peak, Saskatchewan field are examples of where this kind of technology has been extensively employed. The passive method commonly known as Steam Assisted Gravity Drainage (SAGD) involves this use of two horizontal wellbores drilled with a few metres of vertical separation. Steam is injected in the upper wellbore at low pressure. The thermal energy reduces the viscosity of the oil

which seeps downward under gravity and is produced through the lower wellbore. Another method of heavy-oil extraction involves the use of large cavity pumps that produce the sand with the oil. A low-pressure wormhole or zone of high porosity is created that draws a slurry of foamy oil and sand to the wellbore (Chen et al., 2003).

The recovery efficiency of these in-situ methods is not fully understood. The concept of time-lapse seismic monitoring has been introduced in the heavy-oil field in an attempt to image and constrain the problem. It has been well established that the introduction of steam and higher temperatures into a reservoir changes the fundamental rock properties. The changes in these properties are significant enough to alter the seismic response. The applications of seismic analysis and monitoring for hydrocarbon production in Western Canada have been discussed by Pullin et al. (1987), de Buyl (1989), Lines et al. (1990), Matthews (1992), and Schmitt (1999).

The Pikes Peak field, operated by Husky Energy Ltd., has been the focus of seismic monitoring. In this study, four techniques for seismic detection of steam and heat fronts were examined over a portion of the field (Watson et al., 2002). These include:

- Differencing of reflectivity functions for the monitor and base surveys.
- Differencing of acoustic impedance estimates for the monitor and base surveys.
- Comparison of interval P-wave traveltimes for the monitor and base surveys.
- Estimation of  $V_P/V_S$  variation from multicomponent data.

The results of these approaches are compared and contrasted as a means of detecting steam fronts and heated zones within the Waseca reservoir. The use of the monitor and base surveys is very sensitive to the calibration of the coincident lines. Amplitude scaling and phase matching between the base and monitor survey need to be considered. For interpretation or interval travelttime analysis, the different bandwidth and potential tuning effects must be recognized. The base and monitor surveys do allow geoscientists and engineers to see changes with time. The single multicomponent survey provides a snapshot in time of the subsurface reservoir. With the use of converted-wave interpretation and inversion techniques (Zhang, 2003), a multicomponent survey provides a more constrained evaluation of the reservoir than normal vertical array data. As converted-wave technology advances and is proven, it is becoming a more popular, feasible and economical method to acquire seismic data.

The integration of reservoir engineering data with the time-lapse seismic lines provides a validation of the reservoir surveillance techniques using seismic data. Knowing when and where wells were drilled in the vicinity of the time-lapse seismic surveys is essential to understand the seismic response. Associated well data, such as steam injection, heavy-oil and water production rates from these wells, are an equally important part of the data integration.

The hydrocarbon trap formation and reservoir stratigraphy at Pikes Peak are interpreted and discussed to provide a broader understanding and context for the seismic investigation. The interval travelttime of a deep Devonian salt explains the present day

structure of the Cretaceous reservoir and where the risk of water in the reservoir is highest. The  $V_p/V_s$  variation estimated from multicomponent data provides a method to delineate sand-rich reservoir from shale (Watson and Lines, 2003).

## **1.2 Previous related work**

Heavy-oil fields have been evaluated using geophysical data for several years. Most methods are based on the ideas originated by Nur (1982) who demonstrated that P-wave velocity is significantly lowered with temperature increase in heavy-oil saturated sands. Nur's results have led to many time-lapse seismology projects in Western Canada heavy-oil fields. Nur and Wang (1989) were the editors of a Geophysics reprint series that was dedicated to the investigation of seismic and acoustic velocities in reservoir rocks.

The applications of seismic monitoring for Athabasca oil sands were discussed by Pullin et al. (1987), de Buyl (1989), Lines et al. (1990), and Matthews (1992). Further advances for seismic monitoring of enhanced oil recovery at Cold Lake, Alberta were made by Eastwood (1993), Eastwood et al. (1994), Isaac (1996), and Sun (1999).

The release of the Pikes Peak data to the University of Calgary, the acquisition of the March 2000 vertical array and multicomponent seismic and microphone data, and the acquisition of a September 2000 multicomponent vertical seismic profile (VSP) have provided the basis of several research papers and theses for this producing heavy-oil field. Hoffe et al. (2000) discussed the acquisition and processing of the multicomponent data. Dey et al. (2000) examined the ability to suppress near surface noise on geophone data using microphone data. Stewart et al. (2000) examined the use of recording

multicomponent data on cables placed in the bottom of a small lake near the VSP acquisition site. Brittle et al. (2001) used the March 2000 data to analyse vibroseis deconvolution. Xu (2001) and Osborne and Stewart (2001) reported on the acquisition and processing of the VSP data. Newrick et al. (2001) presented an investigation of seismic velocity anisotropy at Pikes Peak using the VSP data. Hedlin et al. (2001) examined the effect of seismic attenuation through the steamed reservoir. Downton et al. (2001) examined the feasibility of Amplitude Versus Offset (AVO) time-lapse analysis. Zhang (2003) performed a joint inversion on the P-P and P-S (converted-wave) data. Zou et al. (2002) has modelled the seismic response of a reservoir simulation and shown similarities to real data analysis by Watson et al. (2002).

Van Hulten (1984) provided a comprehensive geologic framework for the Waseca Formation in and around the Pikes Peak field. Sheppard et al. (1998) presented a paper at the UNITAR Conference in 1998 providing primarily a reservoir engineering overview of Husky's thermal project at Pikes Peak. Wong et al. (2001) discussed the issue of bottom water in the Pikes Peak reservoir and how the field development can be extended into these areas where water saturated sands underlie heavy-oil saturated sands.

Multicomponent technologies have been proven in other areas of Western Canada and are applicable to monitoring and interpreting the heavy-oil reservoir at Pikes Peak. Miller (1996) published a Masters thesis on multicomponent seismic data interpretation over carbonate (Lousana, Alberta) and clastic (Blackfoot, Alberta) oil and gas fields. Stewart et al. (1996) and Margrave et al. (1998) published papers where multicomponent

interpretation provided a basis to discern sand-rich reservoir from shale at Blackfoot, Alberta.

The use of geophysical data for reservoir interpretation, surveillance and monitoring has gained acceptance in the oil and gas industry. Justice (1992) and Sheriff (1992) discuss the petrophysical and geophysical basis for reservoir surveillance using primarily seismic technology. Richardson and Sneider (1992) evaluate the roles of geophysicists, geologists and engineers during the various stages in the life of an oil or gas asset. Wang and Nur (1992) summarize their previous rockphysics research for reservoir surveillance applications.

### **1.3 The Pikes Peak Field**

#### **1.3.1 Location**

Husky Energy Ltd. operates the Pikes Peak Heavy-oil Field in West Central Saskatchewan. The field is located 40 km east of Lloydminster, Saskatchewan (Figure 1-1). In the area around Pikes Peak heavy oil is produced in-situ (from the subsurface) from Mannville sands. Several other major heavy-oil fields surround Pikes Peak field. These heavy-oil producing fields include: Celtic, Standard Hill, West Hazel, Tangleflags, Lashburn, Golden Lake and Gully Lake. Diluents (condensate or naphtha) are used to dilute the viscous heavy oil so it can be transported via pipelines to upgraders or refineries. The oil produced from Pikes Peak is piped to Husky's upgrader located on the east side of the town of Lloydminster. The upgrader handles 65 000 - 75 000 barrels of heavy oil daily from the Lloydminster region. It takes the low grade and viscosity oil

through a thermal cracking process breaks the crude into fractions and by-products (petroleum coke, sulphur and synthetic blend) (Husky Energy, 2002).

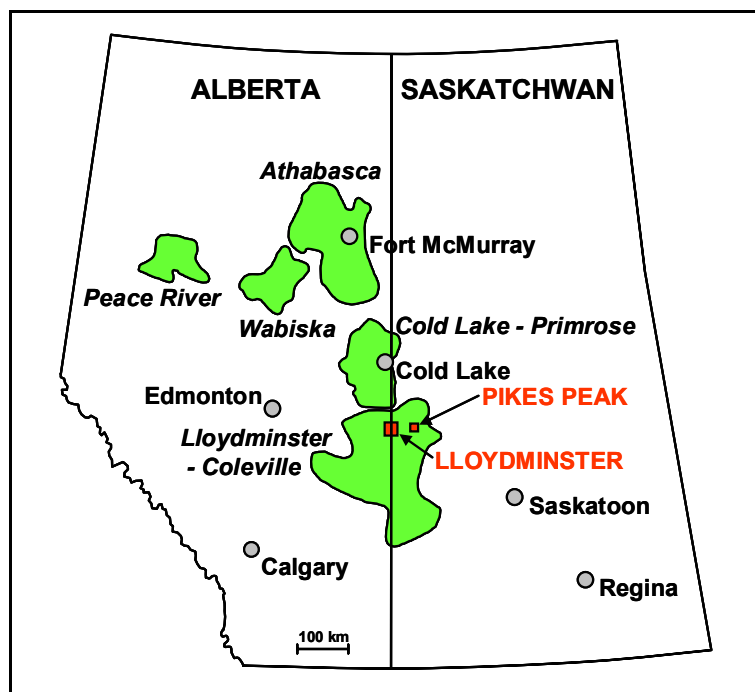


Figure 1-1: Map of major heavy-oil deposits of Alberta and Saskatchewan

### 1.3.2 Field History

The Pikes Peak field was initially discovered in November 1970 with the A09-01-50-14W3 well (Van Hulten, 1984). This well targeted a deeper reservoir interval but encountered nine meters of heavy-oil saturated sands in the Waseca Formation. Throughout the 1970's drilling delineated the extent of the prolific Waseca sands in the Pikes Peak area.

Husky Energy Ltd. has operated the Pikes Peak heavy-oil field since 1981. The field has yielded over 42 000 000 barrels of heavy oil. Wells have been drilled for field delineation, production, steam injection, observation, and water disposal. Nearly 300

wells have been drilled at Pikes Peak to develop the Waseca reservoir. Figure 1-2 is a chart of the field production history. In 1982 and 1983 the field infrastructure was initially built and production rates started off at 5 000 barrels/day (bbl/d) of oil. By the late 1990's production had climbed to 10 000 bbl/d. The number of wells on production is shown on the chart (right axis). The yield per well has decreased over the life of the field because the sweet spots (highest quality, thickest sands and no bottom water) were exploited in the earlier stages of development.

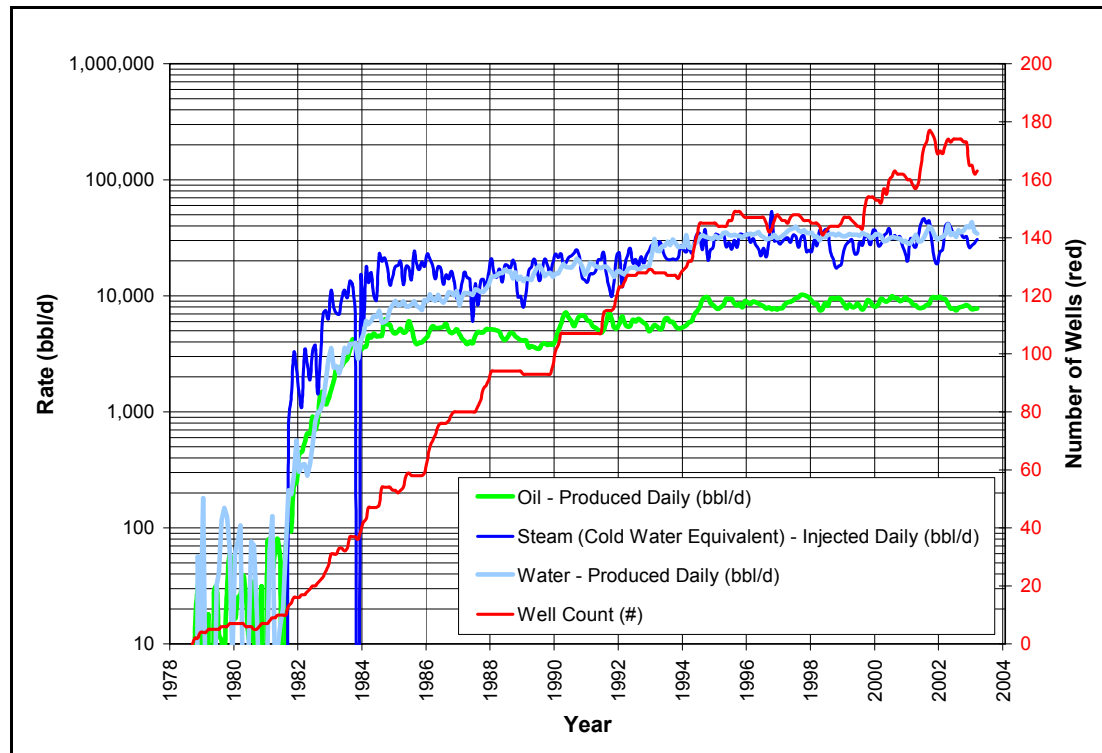


Figure 1-2: Production history from the Pikes Peak Waseca Formation.

Steam technology has been used to assist recovery. With steam injection the effective viscosity of the oil is reduced and the mobility is increased in the reservoir with the injection of high temperature and pressure steam. Husky has employed several different

steam injection techniques over the life of the field (Shepherd et al. 1998). The oil is produced either from neighbouring wellbores or through the same wellbore used for injection (cyclic). Figure 1-2 also shows the volumes (bbl/d) of water (steam) injected and produced back with the oil. In the later stages of the field production, Husky has been forced to inject and produce three times more water than oil produced. Steam-generation and water-separation facilities and pipelines are required to handle these large volumes of non-revenue generating fluids. The produced water is injected in (non-hydrocarbon bearing) Lower Cretaceous sands below the Waseca reservoir interval.

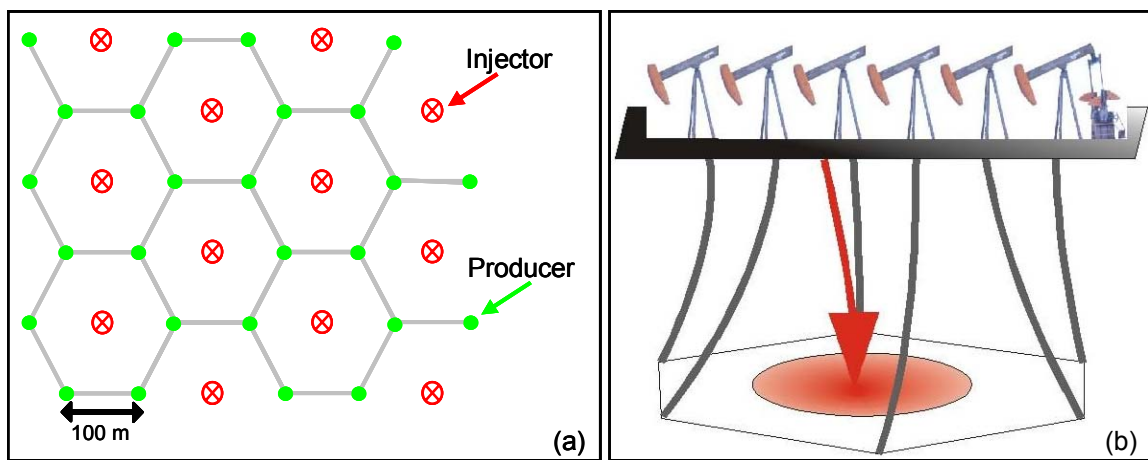


Figure 1-3: (a) Map view of inverted 7-spot honeycomb pattern and (b) Conceptual 3D view.

Steam drive technology has been one method used to enhance recovery. To optimize the effect of the steam injection and maximize the recovery efficiency wells were drilled in an inverted 7-spot honeycomb pattern (Figure 1-3a) over the field. A conceptual drawing of the 7-spot pattern is shown in Figure 1-3b. The central well is used to inject the high temperature and pressure steam while the perimeter wells are produced. The reservoir is heated in the area around the injector. The heavy oil has its viscosity reduced

and flows much more freely to the producing wellbores. Conversely every producing wellbore has three neighbouring injection wells. On the field-scale, the honeycomb geometry requires one injector for every two producers. After some time the steam breaks through to the producing wells. This effect is inevitable but is not desired because it creates a direct path from the injector to the producer leaving areas of unswept reservoir behind. Pressure gradients, which assist fluid flow, are set up between the injectors (high pressure) to the producers (low pressure).

Two other methods that have been applied at Pikes Peak are cyclic steam simulation (CSS) and recently Steam Assisted Gravity Drainage (SAGD). For CSS the same wellbore is used for both steam injection and producing the fluids. The time period of injection can vary from weeks to months depending on pressures and on how much the reservoir is being accessed by the steam. After a period of soaking the well is converted to a producer. Typically a full cycle takes 200 - 500 days (Wong et al., 2001). The earlier cycles are shorter because heavy oil produced is closer to the wellbore. The distance to access the heavy oil and the time to produce it increases with each cycle. SAGD makes use of two horizontal wellbores in the reservoir with a few metres of vertical separation. Steam is injected into the upper well and the combination of steam and gravity allows the heavy oil to be produced from the lower wellbore.

Husky has reported (Wong et al., 2001) that in areas where there is no bottom water in the Waseca reservoir they have seen recoveries of up to 70 percent of the original oil in place. Typically the wells are put on CSS and then converted to steam drive. For the

first three cycles of CSS the steam-to-oil ratio (SOR) tends to be a favourable 1.4 - 1.8  $\text{m}^3/\text{m}^3$  and they see recoveries of 25 - 35 percent. In the fourth cycle of CSS the SOR jumps up to 3.0  $\text{m}^3/\text{m}^3$  because the near wellbore heavy oil has already been recovered. With the conversion to steam drive they see a cumulative SOR of 3.3  $\text{m}^3/\text{m}^3$ . The higher the SOR the less economic it is to get the heavy-oil resource out of the reservoir. These results were seen on 150 non-bottom water wells in the core of the field.

As Husky moves forward in development they need to deal with bottom water on the edges of the field. There is a large heavy-oil resource in the Waseca above the bottom water. The risk of bottom water is that it can steal a lot of the heat and energy put into the reservoir during steam injection. Pilots in the 1980s and 1990s indicated that they would be able to operate CSS successfully in areas with thin bottom water (less than 5 m). Compared to wells without bottom water, wells with bottom water require longer cycles and a higher steam injection rate to achieve similar production. In test wells, with thin bottom water, they have seen comparable recoveries with a slightly less favourable SOR of 1.9 - 2.3  $\text{m}^3/\text{m}^3$  after three cycles of CSS. The SOR rises to 3.6  $\text{m}^3/\text{m}^3$  for the fourth cycle. Chapter 2.2 discusses the structure of the Pikes Peak field and some of the controls on presence of bottom water in the Waseca.

### 1.3.3 Reservoir Parameters

Table 1-1 provides a summary of the key reservoir parameters.

Table 1-1: Summary of Waseca reservoir parameters at Pikes Peak (after Wong et al., 2001)

Depth	475 - 500 m
Maximum Dip	4.5°
Net Pay Thickness (m) – range	5-30 m
– median	15 m
Porosity – range	32-36 %
– median	34 %
Permeability – range	1-10 Darcies
– median	5 Darcies
Oil Saturation	78 – 92 %
Initial Reservoir Pressure	3350 kPa
Initial Reservoir Temperature	18 °C
Oil Formation Volume Factor	1.022 m <sup>3</sup> /m <sup>3</sup>
API Gravity	12.4 °
Oil Density	985 kg/m <sup>3</sup>
Dead Oil Viscosity @ 18 °C	25 000 mPa.s
Solution Gas:Oil Ratio	14.5 m <sup>3</sup> /m <sup>3</sup>
Mineralogy:	
Quartz	92 %
Feldspar	3 %
Kaolinite	3 %
Other	2 %

### 1.4 Data

During the 25-year development of the Pikes Peak field various types of data have been collected. Most of the data including seismic, well log and production data were provided by Husky Energy. Figure 1-4 is a map of the Pikes Peak field.

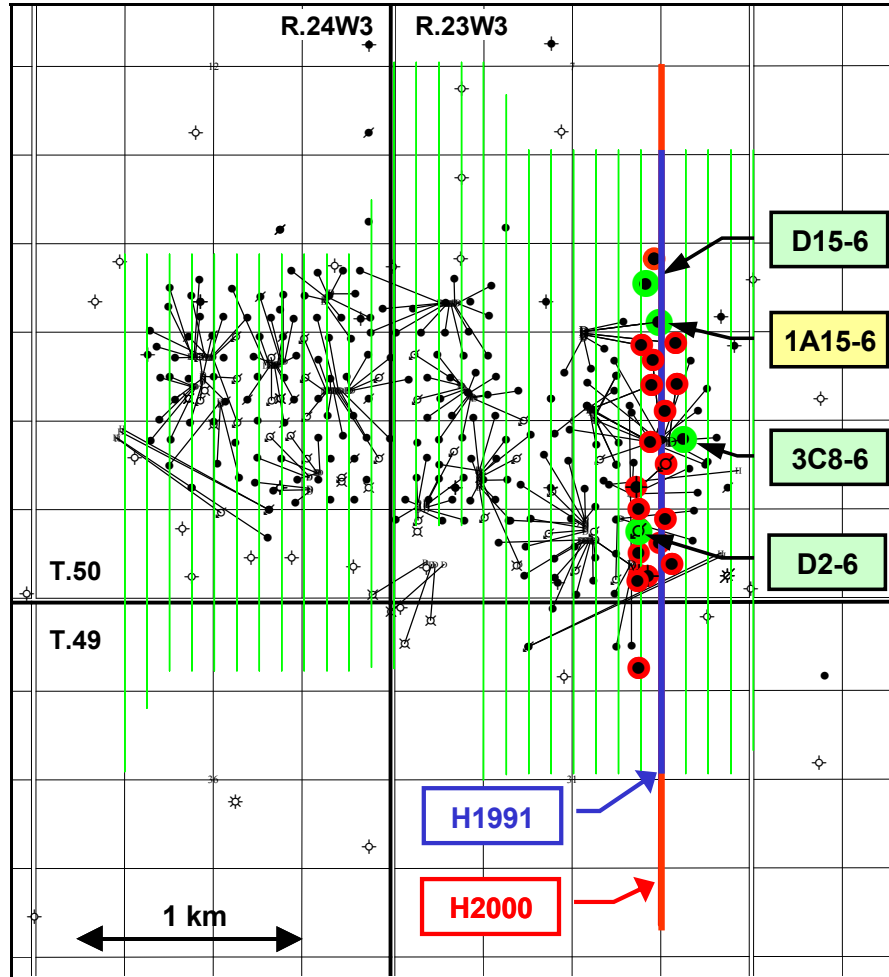


Figure 1-4: Map of the Pikes Peak Field.

#### 1.4.1 Geological data

Of the approximate 300 wells in the Pikes Peak field only a small subset were chosen for this integrated study. 24 wells were selected because the bottom-hole locations were approximately within 110 m of the seismic lines that were interpreted and analyzed. The 110 m limit was used because the geology can change dramatically over greater distances and the Husky Energy engineers did not anticipate that the effect of steam or heat in the

reservoir would extend further. The largest steam zone radius that they had estimated was approximately 45 m.

Core samples of the Waseca Formation have been retrieved from over 30 wells in the Pikes Peak field. Core data provides the smallest scale observations of the field. Samples of the core retrieved from the well D2-6 were sent to Core Laboratories to investigate various rock and fluid properties. The core analysis and results are discussed in Chapter 2.3.

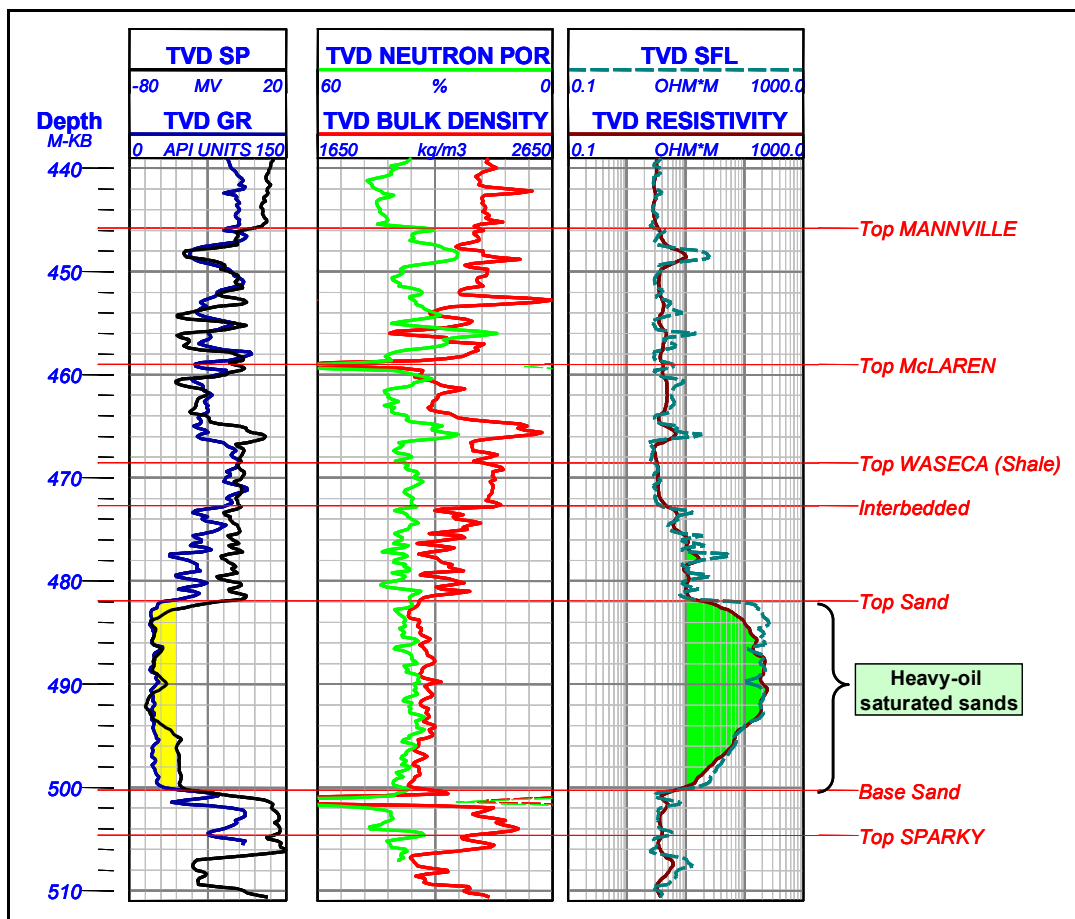


Figure 1-5: Typical log suite used for well log interpretation over the zone of interest. The bottom-hole location of the well 3B9-6 is 87 m east of the time-lapse seismic lines.

Open-hole well log data has been collected in nearly every well in the field. A typical suite of logs typically includes: gamma ray (GR), spontaneous potential (SP), resistivity (deep, medium and shallow focused), neutron porosity, and bulk density. A sample well, 3B9-6, is shown in Figure 1-5. The well was drilled deviated, so the logs were corrected from measured depth (MD) to true vertical depth (TVD).

The gamma ray log was primarily used to interpret sand versus shale. The higher resistivity of heavy oil allowed the interpretation of heavy-oil saturated sands versus water saturated sands using the resistivity log data.

The wells of greatest importance to this integrated interpretation were the wells that had sonic and/or bulk density logs collected. In the entire Pikes Peak field only 33 traditional sonic logs have been collected over the Waseca reservoir interval. Three wells with sonic logs (D15-6, 3C8-6 and D2-6) lie within 110 m of the 2D seismic lines. The seismic interpretation and inversion used these wells for synthetic ties and constraining the inversion model building process. Dipole sonic logs have only been run on a couple Pikes Peak wells. The P- and S-wave logs from the well 1A15-6 were used to interpret the converted (P-S) seismic data.

The location, rig release dates and log data collected for each well used in this study is summarized in Appendix A.

#### **1.4.2 Geophysical data**

Husky acquired a 2-D seismic swath survey in 1991 which forms a grid of 29 north-south lines spaced every 100 m (see Figure 1-4). To investigate time-lapse effects and

collect 3-component data the University of Calgary and Husky Energy sponsored by AOSTRA (Alberta Oil Sands Technology Research Authority) returned to the field in March 2000 to acquire a single repeat line on the eastern side of the field. During the acquisition four components were collected: P-wave (vertical and array), SV-wave, SH-wave and experimental surface microphone (Dey et al. 2000) data. A multi-offset VSP was also acquired at the D15-06 well location in September 2000 (Stewart et al. 2000).

Table 1-2: Summary of 2D survey differences at Pikes Peak.

	<b>H1991</b>	<b>H2000</b>
Acquisition date	February 1991	March 2000
2D line length	2.8 km	3.8 km
Data types acquired	Vertical array	Vertical array Multicomponent (3-C) Microphone
Sweep length	6 msec	16 msec
Sweep bandwidth (non-linear)	8-110 Hz	8-150 Hz
Vibroseis points	3 vibrators over 20 m	2 vibrators over 20 m
Sweeps/vibroseis point	4	4
Vibroseis drag length	10 m	No drag
Source interval	40 m	20 m
Receiver group interval	20 m	20 m (array) 10 m (3-C)
Receiver groups	9 geophones over 20 m	6 geophones over 10 m
CDP fold	30	66
Processed bandwidth	14 – 110 Hz	14 – 150 Hz (array & P-P) 8 – 40 Hz (P-S)

The key acquisition and processing differences in the two seismic surveys are summarized in Table 1-2. The most significant difference between the two surveys was the final bandwidth. The March 2000 data contains the higher frequency data mainly because the vibroseis source was broader bandwidth. The time-lapse lines are referred to as H1991 and H2000 (array) as shown in Figure 1-4. H2000 (3.8 km) extends to the north and south beyond H1991 (2.8 km).

All versions of the seismic lines were processed at Matrix Geoservices Ltd. in Calgary using very similar workflows in May 2000. Details of the processing flow used by Matrix are provided in Appendix B for each line analysed in this thesis.

Some differences can be expected in the two time-lapse sections not only because of the production and steam injection history in the reservoir. The acquisition parameters and field conditions were different. For example, the H1991 lines used a vibroseis sweep of 6 seconds over the frequency range of 8 - 110 Hz. The H2000 line was swept for 16 seconds over 8 - 150 Hz. Additional noise is expected on the H2000 line because many more pump jacks were in operation during acquisition than in 1991. The increase of fold from 30 to 66 helps to stack out more of this noise. The difference in coupling of geophones is unknown but should have been mitigated by having both surveys acquired in the winter months when the geophones tend to be frozen in the ground.

The final trace spacing was 10 m for the array data. Figures 1-6 and 1-7 show the reflectivity sections (vertical array) for H1991 and H2000 lines, respectively. The Waseca and Sparky reflectors are shown on both sections with the Devonian reflector

being deeper at about 700 ms. Evidence of the higher frequency content in H2000 can be seen directly on the seismic section when compared to H1991. The vertical (P-P) and radial (P-S) component sections from the converted-wave data are shown in Chapter 5.

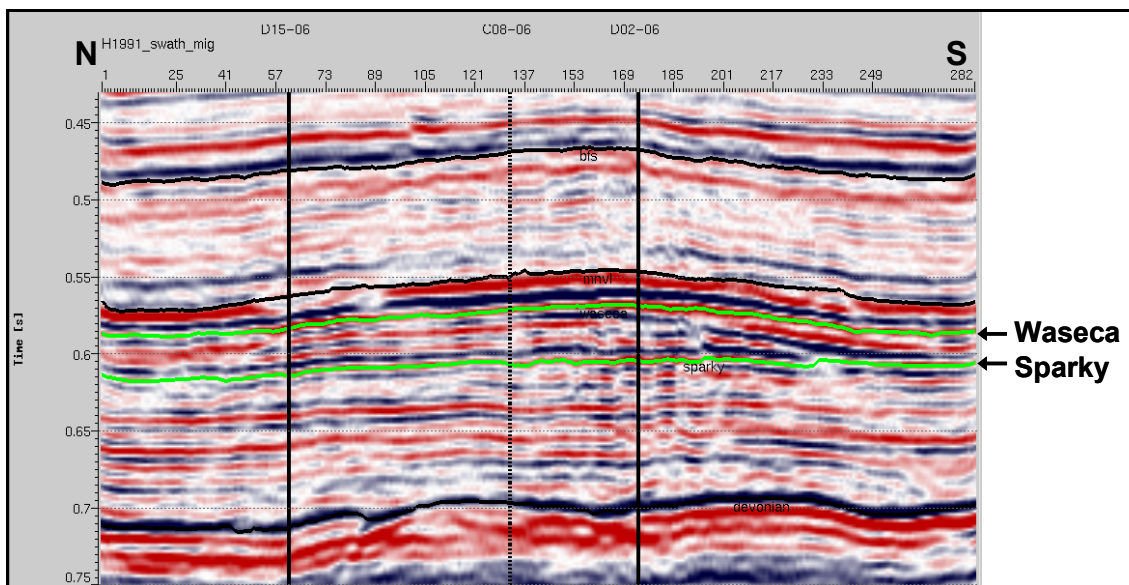


Figure 1-6: H1991 reflectivity section.

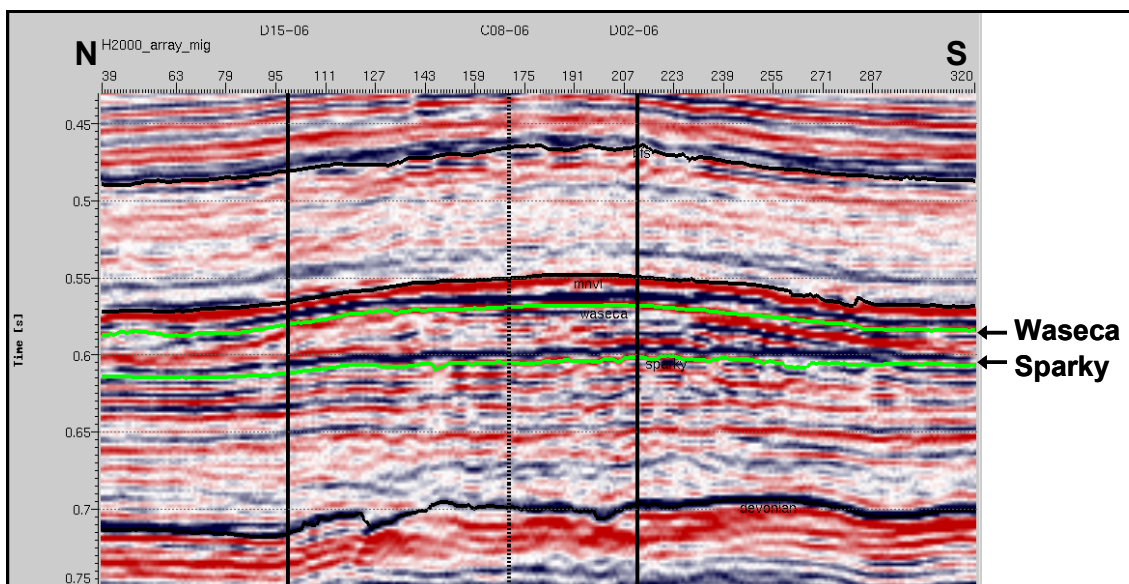


Figure 1-7: H2000 (vertical array) reflectivity section.

### 1.4.3 Engineering data

Engineering data are critical in order to understand the seismic response of the Waseca reservoir to the injection of high temperature steam and related production. Unlike well and seismic data which are spatially sampled in a multi-dimensional manner, engineering tends to be single point data. Husky engineers and geologists provided important numbers to complete the picture of field activities along the two time-lapse seismic lines. These individual well statistics included: perforation intervals, net pay thickness, production volumes, injected steam volumes, produced water volumes, reservoir pressure and temperature. With these data, the engineers were able to predict a steam-zone radius around each wellbore in February 1991 and March 2000.

The steam-zone radius was calculated assuming the steam zone forms on an inverted cone shape ( $V_C = \pi r^2 h / 3$ ) in the reservoir. Taking the porosity ( $\phi$ ), oil saturation ( $S_O =$  original saturation – residual saturation), and cumulative volume of oil ( $V_O$ ) produced to the given date the cone volume,  $V_C = V_O / (\phi * S_O)$  was calculated. With the sand net pay ( $h$ ) an estimate of the radius ( $r$ ) at the top of the steam zone was back-calculated.

A summary of the steam zone radii, pressure, temperature, production and injection data for each well adjacent to the H1991 and H2000 seismic lines are provided in Appendix C (Tables C-1 and C-2).

Production and injection data for individual wells, similar to Figure 1-2, provide a history of the performance and status changes. Without these reservoir data none of the geophysical interpretations could be properly evaluated and validated.

## **1.5 Software and Hardware**

Several applications were used to perform modeling, analysis, interpretation and integration of data at Pikes Peak.

GMAPlus was used for well-log data quality control, synthetic forward modeling, and stratigraphic correlations and marker picks. Seismic ties, interpretation, and inverse modeling and were done in Jason Geoscience Workbench. The time-lapse analysis of the reflectivity and inverted seismic data was performed using the Pro4D module in Hampson-Russell Software. CREWES' MATLAB code 'synth' was used to create the converted-wave offset model. IHS Accumap was used to create field maps and collect well and field data (well logs, industry markers, production and injection volumes, and general well information).

Charts and figures were created using Microsoft Excel. Word and PowerPoint were used to document and present the results of this thesis work.

Sun Unix workstations and Windows-based personal computers were used to run the various software programs.

## Chapter 2

### Reservoir Characterization

#### 2.1 Stratigraphy

The preserved geologic section of the Lloydminster area is relatively simple compared to the rest of the Western Canadian Basin. The stratigraphic chart (Figure 2-1) summarizes the age, name, lithology and approximate depth from surface of the significant stratigraphic units in west-central Saskatchewan.

AGE / GROUP		FORMATION	LITHOLOGY	APPROX. DEPTH	
QUATERNARY		GLACIAL DRIFT			
CRETACEOUS	UPPER	JUDITH RIVER			
		LEA PARK		- 150 m -	
		<b>COLORADO GROUP</b>	SHALE	- 300 m -	
		SECOND WHITE SPECS BASE OF FISH SCALES			
	LOWER	<b>MANNVILLE GROUP</b>	VIKING		
			JOLI FOU		- 450 m -
			COLONY		
			MCLAREN		- 475 m -
			<b>WASECA</b>		- 510 m -
			SPARKY	SANDSTONE & SHALE	
			GENERAL PETROLEUM		
			REX		
			LLOYDMINSTER		- 550 m -
			CUMMINGS		
DINA		- 650 m -			
DEVONIAN	SASK. GROUP	DUPEROW	DOLOMITE		
	MANITOBA GROUP	SOURIS RIVER		- 825 m -	
	ELK POINT GROUP	<b>PRAIRIE EVAPORITE</b>	EVAPORITE	- 950 m -	
		WINNIPEGOSIS			
		ASHERN		- 1050 m -	
CAMBRIAN	DEADWOOD		- 1600 m -		
PRECAMBRIAN					

Figure 2-1: Generalized Stratigraphic Chart for the Pikes Peak area (after Core Laboratories Stratigraphic Chart for Saskatchewan).

The top of the Precambrian basement has been penetrated at depths of approximate 1600 m. The basement dips to the west-southwest and reaches depths of over 4000 m in the deepest parts of the Basin near the Foothills of Alberta. Preserved above the basement are primarily Devonian and Cretaceous age formations. The dominant lithology of the preserved Devonian formations is limestone and dolomite with the exception of the Prairie Evaporites. This unit is composed of salt. The Prairie Evaporites' differential preservation was critical to the formation of the hydrocarbon trap at Pikes Peak (Chapter 2.2). There is a 250 Ma hiatus which is represented by the boundary between the Devonian and Cretaceous. This boundary is commonly referred to as the PreCretaceous Unconformity (PCU). Deposited on the PCU is a mixture of sand and shale cycles that make up the Lower Cretaceous Mannville Group. Van Hulten (1984) suggests that the sand-shale cycles observed in the stratigraphy of the Mannville were influenced by minor relative sea-level variations. The paleogeography was very flat and small changes in relative sea-level could quickly change the depositional setting. The Pikes Peak field produces from the heavy-oil bearing Waseca Formation of the Lower Cretaceous Mannville Group.

Van Hulten (1984) describes two different facies types within in the Pikes Peak area, a regional facies and a channel or incised valley facies. The Pikes Peak Field is centered over this subsurface incised valley (see Figure 2-2). The seismic data (H1991 and H2000) were mainly acquired over the incised valley facies. Van Hulten suggested that the channel flowed from south to north. The joint inversion work by Zhang (2003) provides further evidence to support the north to south flow. The simultaneous (P-P – P-

S) inversion results exhibit a clinoform geometry suggesting northward prograding sequences. Another source of data to support the south to north flow is dipmeter logs which were run in a few wells at Pikes Peaks. Interpreted dipmeter logs have the greatest frequency of beds dipping in a northeast orientation.

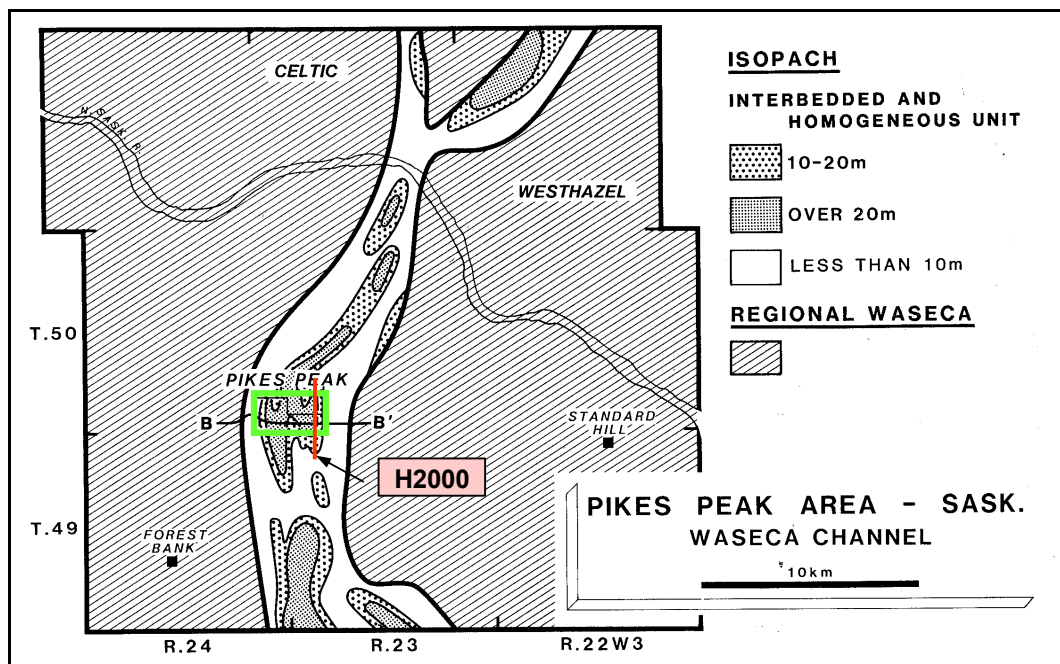


Figure 2-2: Waseca incised valley trend in the Pikes Peak area with annotations of the heavy-oil field and the H2000 seismic line (after Van Hulten, 1984).

A simplified stratigraphic chart of the incised valley facies is shown in Figure 2-3. Van Hulten mapped three discernable units which he identified and described from core. They are:

1. a homogeneous sand unit
2. an interbedded sand and shale unit, and
3. a sideritic silty shale unit.

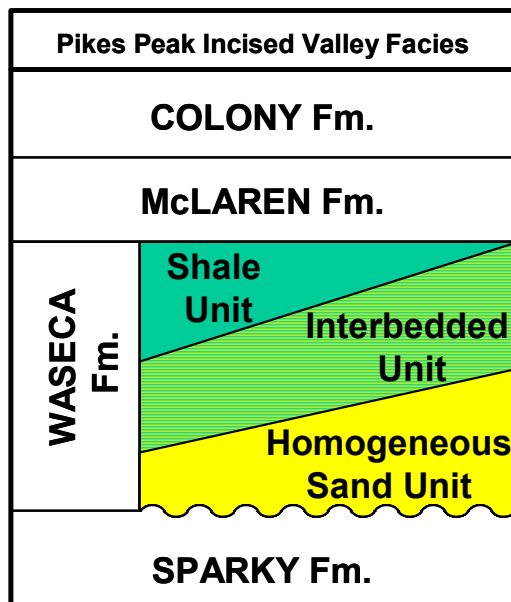


Figure 2-3: Waseca incised valley facies at Pikes Peak (after Van Hulten, 1984).

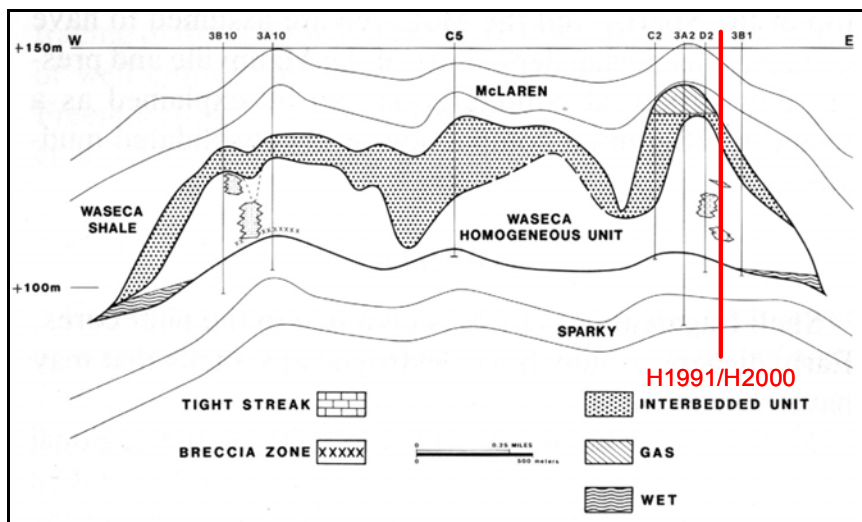


Figure 2-4: West-east structural cross section through Pikes Peak (Van Hulten, 1984).

Figure 2-4 is a west-east cross-section created by Van Hulten and shows the relationship of the three units and how they vary laterally. The cross-section is oriented perpendicular to the incised valley trend. The Waseca interval is underlain by the Sparky

Formation and capped by the McLaren. The core of the field is dominated by the homogeneous sand and interbedded units. The shale unit thickens at the edges of the incised valley. Van Hulten interprets that the homogenous sand unit was deposited as an amalgamation of migrating point bars within the incised valley. The interbedded sand and shale units may represent the gradual abandonment phase of the valley system.

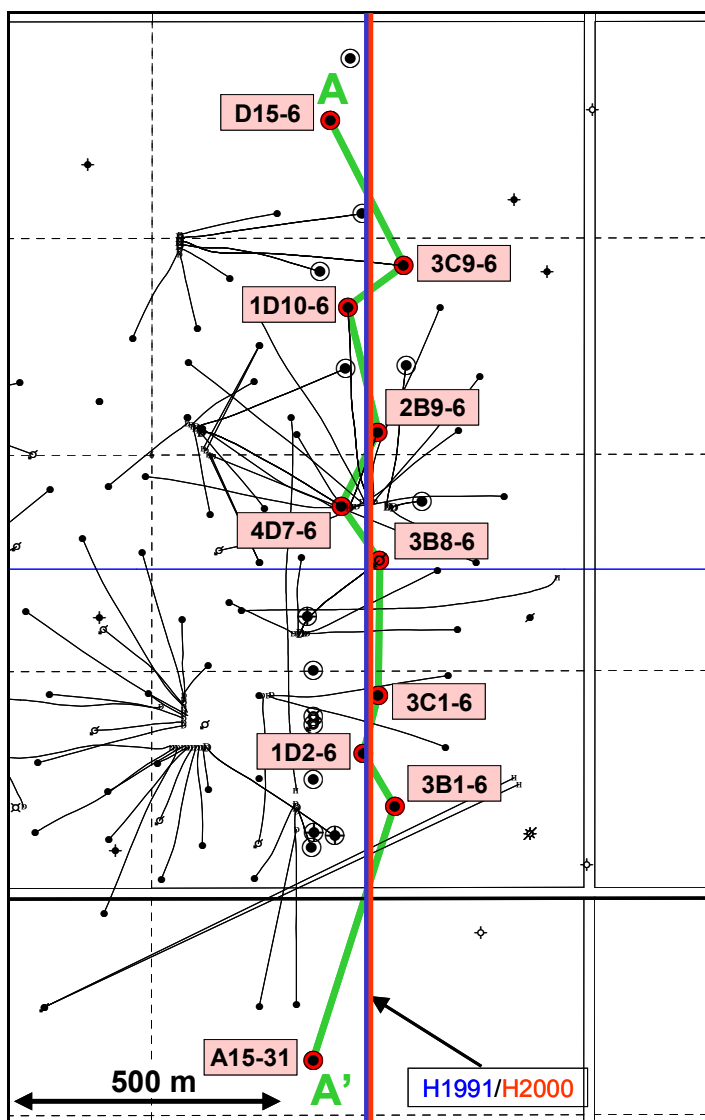


Figure 2-5: Map of the east side of the Pikes Peak field with cross-section A-A' marked.

Using Van Hulten's facies work as a template, the incised valley facies were interpreted for the 24 wells adjacent to the H1991 and H2000 seismic lines. The stratigraphic cross-section A-A' was constructed using 10 of the 24 wells (Figures 2-5 and 2-6) on the east side of the incised valley trend. The cross-section has a north-south orientation, parallel to the incised valley trend. A coal marker, above the Waseca, at the top of the McLaren Formation is present in every well and used as the stratigraphic datum. The coal marker represents a time marker when the paleotopography would have been flat.

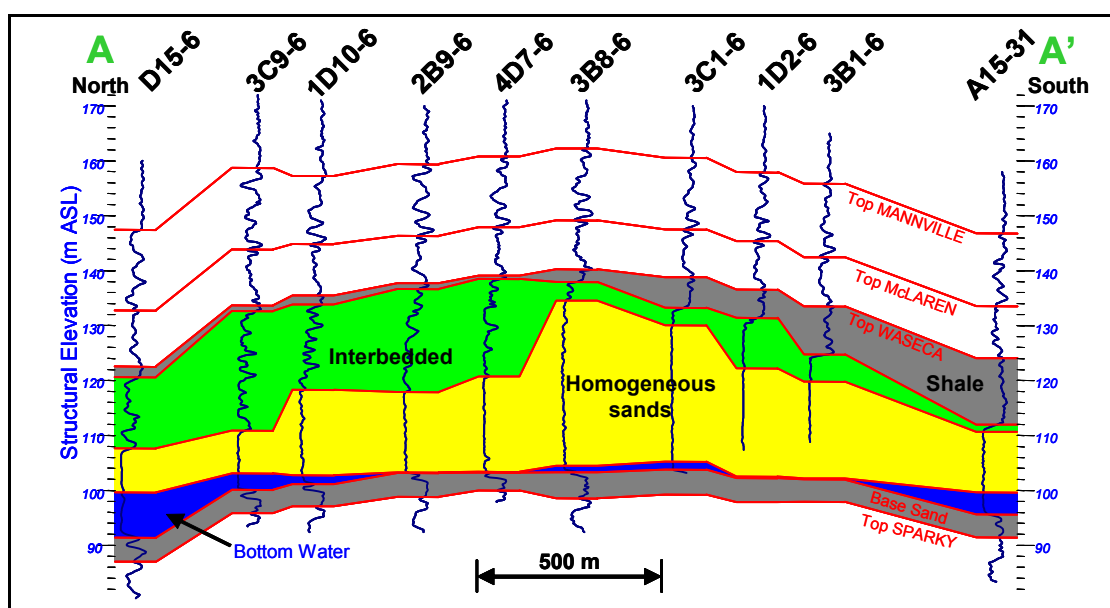


Figure 2-6: Structural cross-section A-A' constructed using gamma ray logs from 10 wells adjacent to H1991 and H2000. Note: the vertical exaggeration is approximately 15 times.

Van Hulten's cross-section and B-B' show how the homogeneous sand is present in every well at the base of the Waseca. The sand is overlain by the interbedded unit and then the shale unit. The shale unit generally thickens towards the south and the

interbedded unit thickens to the north. The location of the northward prograding sequences, as seen by Zhang (2003), suggests that the sand and shale of the interbedded unit are responsible for this depositional geometry that can be imaged with seismic data. Within the Waseca interval, the reflectivity sections (Figures 1-6 and 1-7) show different responses on the southern and northern ends that are related to thicker shale and interbedded units, respectively.

### **2.1.1 Homogenous Sand Unit**

The homogeneous sand unit is the main target for development and the basis for net pay measurements. It is the basal unit of the Waseca Formation and ranges in thickness from 0 – 30 m. As shown in Table 1-1, it is dominantly quartz with smaller fractions of feldspar and kaolinite. The porosity ranges from 30-35 percent and the permeability ranges from 5 – 10 Darcies. The unit is nearly continuous sandstone bedding with minor shale brecciated (discontinuous) beds. Van Hulst observed some planar crossbeds in core but this unit has a massive appearance due to the heavy-oil saturation which makes it difficult to see sedimentary structures. In some wells there are some sideritic or calcite cemented zones or tight streaks within the homogeneous sand. An example of a cemented tight streak is shown in Figure 2-14 with the temperature log in well 6A2-6. These zones can range from a few centimetres up to a few meters in thickness. The sands were cemented early in the diagenetic (burial) process shortly after being deposited. The residual porosity is so low in this calcite cemented zones that there no hydrocarbons or

water were emplaced in this tight rock. Well log correlations suggest that the lateral extent of these zones is up to 100 m.

On logs, such as 3B9-6 in Figure 1-5, the homogeneous sand unit is identified most easily with the blocky low gamma ray response (less than 30 API units – low radioactivity). The SP curve indicates excellent permeability with a large inflection to the left. The neutron and density porosity logs tend to have very little separation and lie between 30 - 35 percent porosity. The resistivity response in the homogeneous sand unit can vary from being very high (20 - 300 ohm·m) when saturated with heavy oil to very low (< 10 ohm·m) when saturated with bottom water. The calcite zones do not tend to affect the gamma ray response but the neutron and density porosity tend to zero. The resistivity logs can rise above 300 ohm·m in these cemented zones.

The homogenous sand unit has excellent reservoir quality and continuity. There are very few obstructions for the steam to spread out through the reservoir.

### **2.1.2 Interbedded Sand and Shale Unit**

The interbedded sand and shale unit unconformably overlies the homogeneous sand unit (see Figure 2-6). This unit is 0 – 15 m thick. It is characterized by alternating beds of sand and shale that are individually a few centimetres up to a couple metres thick. The interbedded unit tends to have a higher frequency of sand beds at the base and an increasing number of shale beds towards the top. The main sedimentary structures in this unit are parallel laminations. Van Hulten observed some bioturbation that increased

upward through the unit. The sands in the interbedded unit tend to be saturated with heavy oil. In some portions of the field, small pockets of gas are present in the sand beds.

The interbedded unit is characterized with noisy logs (Figure 1-5) responding to the alternating beds of sand and shale. Many of the logging tools do not have the vertical resolution to see the smaller individual beds. As a result the measured log responses are averaged or smeared over these intervals. The gamma ray readings range from 30 - 90 API units. The SP only shows some permeability in the thicker sand beds with minor inflections to the left. The neutron and density logs exhibit a noisy response and separate more than in the homogeneous unit. The resistivity tools reads lower (1 – 10 ohm·m) in the shale intervals and higher (10 – 100 ohm·m) in the heavy-oil saturated sand intervals.

The interbedded sand and shale unit has relatively poor reservoir quality and continuity. The shale beds are a barrier to the flow of steam into and heavy oil out of this unit. The lateral continuity of the sands and shale is unknown. It is difficult to correlate log responses within this unit from well to well with any confidence. Heat would rise into this unit but it is uncertain how much heavy oil can be produced out of it with this kind of reservoir heterogeneity.

### **2.1.3 Shale Unit**

The shale unit caps the Waseca in the Pikes Peak incised valley system (see Figure 2-6). It can be less than a metre and up to 20 m thick. It is described as sideritic shale with no porosity or permeability. Wavy to parallel laminations are the dominant sedimentary structures were observed in core by Van Hulten.

The shale unit log response is also unique. The gamma ray reads 90 - 105 API units (due to the higher radioactivity in the shale). The SP curve suggests that the shale has no permeability. The neutron and density curves separate and are less noisy than in the interbedded zone. The resistivity readings are in the 1 – 3 ohm·m range.

The shale unit has no reservoir quality. It acts as the reservoir seal for the porous and permeable sand units below.

## **2.2 Structure**

The main mechanism that creates the trap at Pikes Peak is the partial dissolution of Devonian aged salts. The familiar name of this salt interval is the Prairie Evaporite (refer to the stratigraphic chart, Figure 2-1). The Prairie Evaporite is a member of the Elk Point group. Regionally, this salt unit ranges in thickness from 0 to 150 thick. It is found approximately 825 meters below surface at Pikes Peak.

Figure 2-7 is a map of the greater Lloydminster area indicating the wells that were used to generate a cross-section of deep wells that penetrated through the Prairie Evaporite (after Van Hulten, 1984). The cross-section B-B' is shown in Figure 2-8.

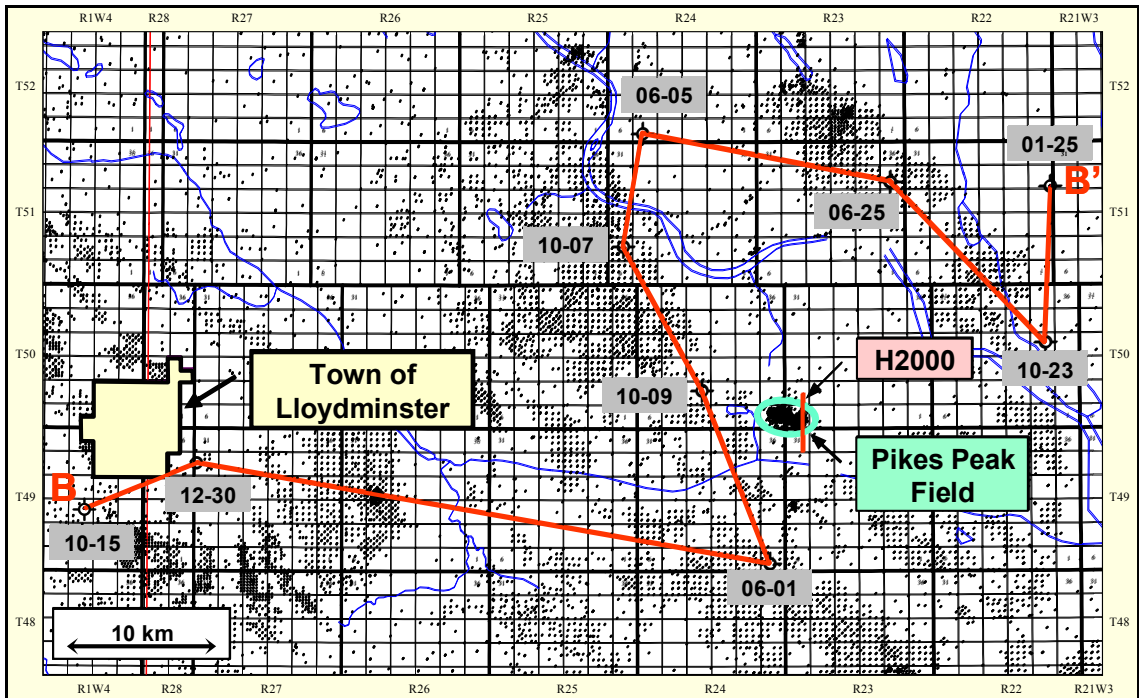


Figure 2-7: Map of the greater Lloydminster area with cross-section B-B'.

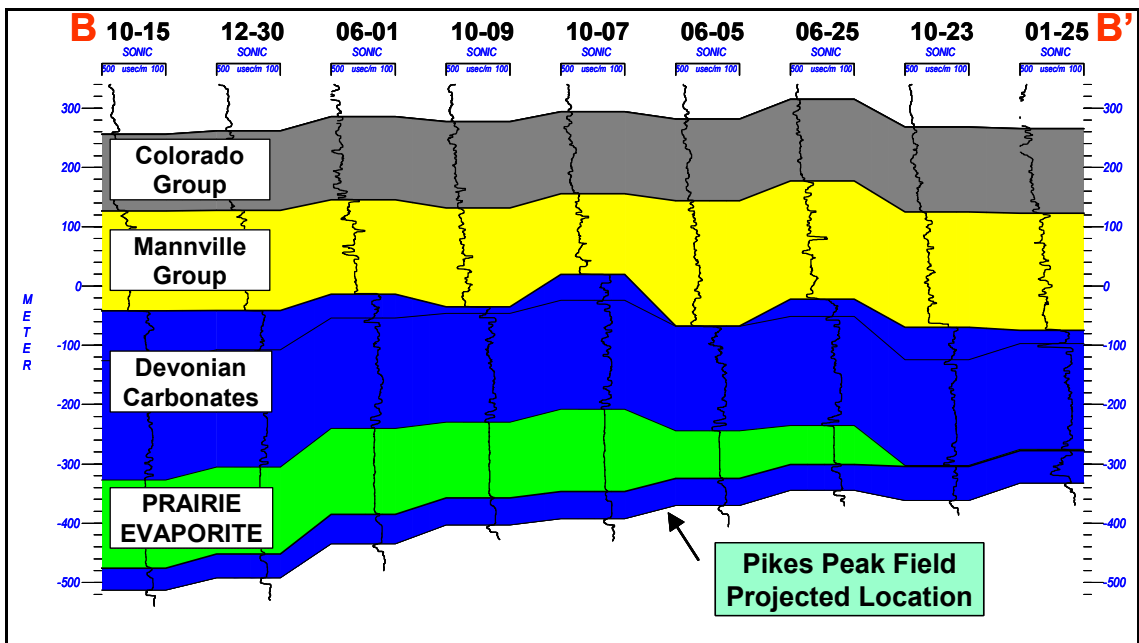


Figure 2-8: Structural cross-section B-B' created with sonic logs (modified after Van Hulst, 1984). Note how the thickness of the Prairie Evaporite varies from 150 to 0 m (west to east) counter to regional dip (east to west).

The cross-section shows how the Prairie Evaporite thins to zero thickness, in a couple wells east of Pikes Peak, from a thickness of 150 m near the Alberta-Saskatchewan border. Salt dissolution is the cause. Dissolution occurred as the salt was exposed to fresh or low salinity water. The controls on the flow of this fresher water is uncertain but may be related to basement involved faulting which can act as a conduit. The effect of this dramatic thinning reverses the dip of the overlying strata which would normally be dipping to the southwest as seen in the strata directly below the Prairie Evaporite. The Precambrian basement, a few hundred metres below the Prairie Evaporite, has this southwest dip straight across to the Alberta Foothills. Locally, in the Lloydminster area, the dip of the Cretaceous strata is northeast which is set up by this differential salt dissolution. These dip reversals create anticlines or a structural high. The Pikes Peak field is situated directly over one of these anticlines and forms a hydrocarbon trap.

No wells within the Pikes Peak field were drilled deep enough to reach the Prairie Evaporite. The closest deep well, 10-09-50-24W3, was drilled 7 km west of the H2000 seismic line. A synthetic 'jump' tie was made to the middle of the H2000 (vertical array) seismic line. This tie is shown in Figure 2-9. The consistency of the geology above and below the Prairie Evaporite throughout the Lloydminster area allows for a high confidence tie. The tie is poorer at the top Devonian because different Devonian formations may subcrop at the Pre-Cretaceous Unconformity over the distance between the well and the seismic line. This subcrop variation can explain the difference in the acoustic response at the Pre-Cretaceous Unconformity. The tie is successful even though the well is seven km west of H2000.

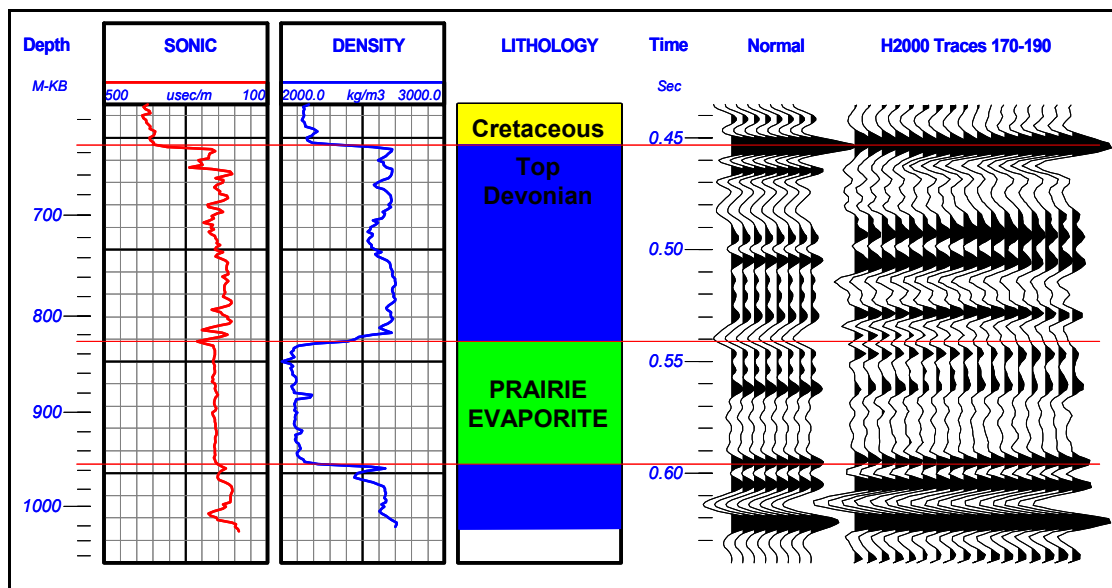


Figure 2-9: Synthetic (normal polarity) tie from well 10-09 to H2000 over the Devonian section.

The synthetic tie was used to interpret the entire H2000 (vertical array) seismic line. (This interpretation could have been effectively done using either the vertical array data or the vertical data from the 3-C survey.) The top and base of the salt unit was interpreted and is shown in Figure 2-10. The base of salt is flat (in travelttime). The top of salt has structural relief. The Waseca reservoir interval is also interpreted. The Waseca interval subtly drapes over the salt structure. This drape suggests that the timing of the salt dissolution was post-deposition of the Waseca. The observed drape higher up in the section (BFS) may be caused by a combination of the salt dissolution and the differential compaction of the sand and shale Waseca interval. The thickest portion of the Waseca is dominated by sand which does not compact as much as where the shale content is higher and the Waseca is thinner.

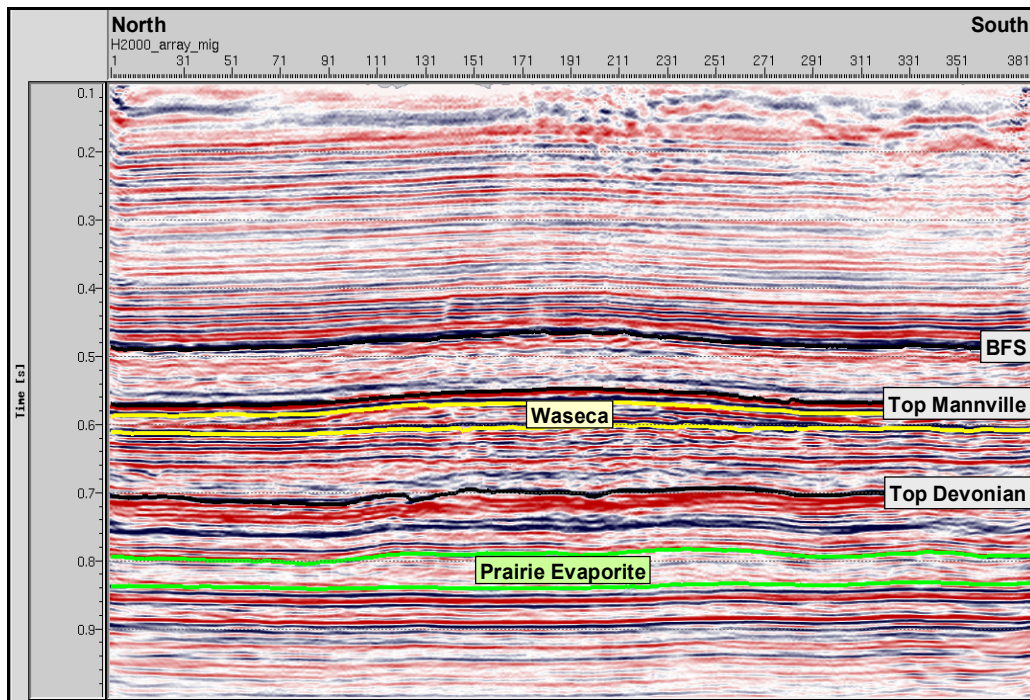


Figure 2-10: H2000 (vertical array) seismic line with an interpretation of the top and base of the Prairie Evaporite and other major horizons.

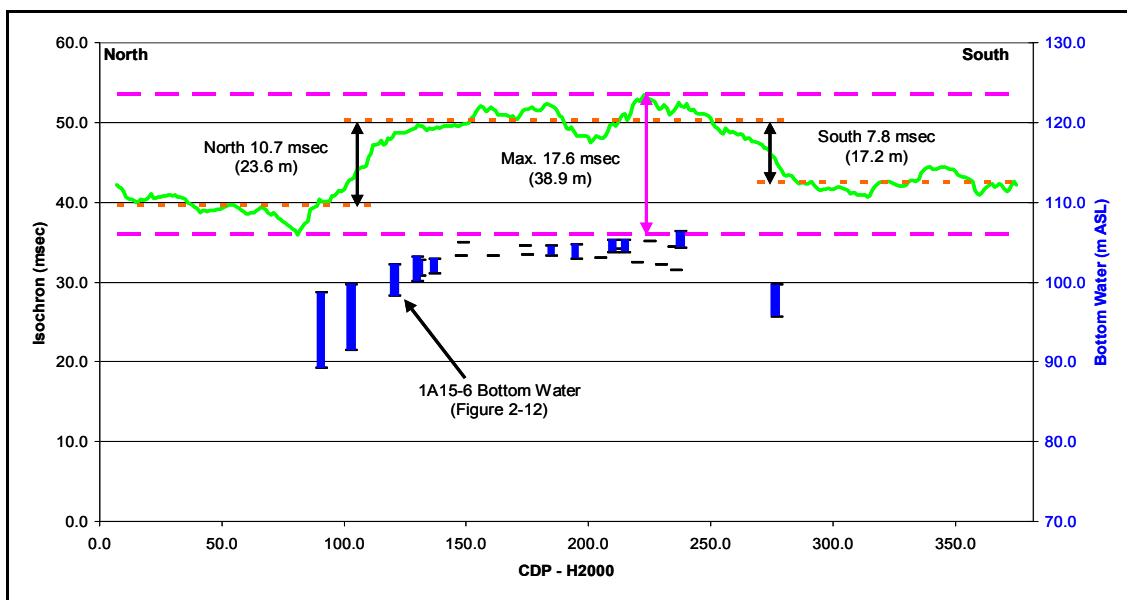


Figure 2-11: Chart of the time thickness of the Prairie Evaporite (left axis) and the structural position of bottom water in the Waseca reservoir in the wells along H2000 (right axis).

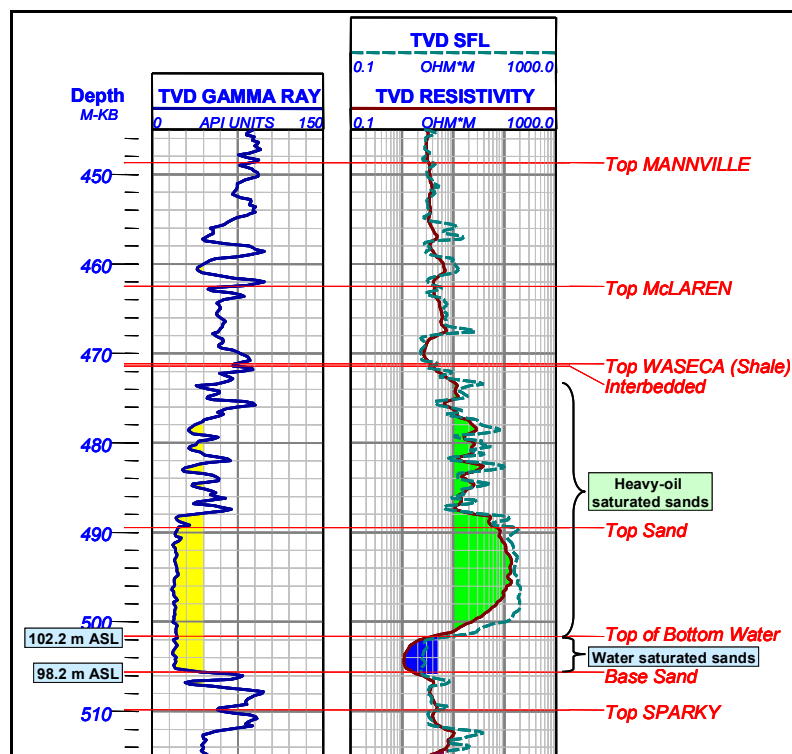


Figure 2-12: Gamma ray and resistivity logs from sample well, 1A15-6, over the upper Mannville. 4 m of bottom water is present at the base of the Waseca sands.

The Prairie Evaporite time thickness or interval travelttime was calculated by subtracting the top of salt travelttime from the base of salt travel time. Shown on the left axis of Figure 2-11 is a line graph of the Prairie Evaporite isochron along the length of H2000. On the right axis is the structural position of bottom water (metres above sea level) in the 24 wells within 110 m of H2000. Where present, the blue bars represent the vertical thickness and structural position of bottom water in each well. For example, the open-hole logs from well 1A15-6 (Figure 2-12) indicate that this well has 4 m of fully water saturated sands at the base of the Waseca. The resistivity logs are used to discern the heavy-oil (high resistivity) saturated from the water (low resistivity) saturated sands.

The most salt preserved is from CDPs 100 to 270. Using the sonic logs from the wells in the regional cross-section A-A' the velocity of the Prairie Evaporite interval was calculated by integrating the sonic transit time. The average interval velocity from these wells was 4412 m/s with a standard deviation of 38 m/s (or less than 1 percent). Taking the product of interval traveltime and the average velocity, the relative thickness of salt removed could be estimated. Over the length of the line the maximum amount salt thickness difference was 17.6 msec or 38.9 m. Compared with the central portion of the line, the north end of the line had an average of 10.7 msec or 23.6 m more salt dissolved. Similarly, the south end of the line had an average of 7.8 msec or 17.2 m less salt than the central portion of the line.

Most of the producing wells are found in the central portion of the line in the structurally highest positions. The three wells outside of the 100-270 CDP range (two to the north and one to the south) are non-producing wells. The presence of bottom water in the Waseca is a concern for reservoir engineers at Pikes Peak. If the steam that is injected into the reservoir connects to the bottom water, the bottom water acts as a thief zone. The steam will preferentially go into the bottom-water zone. The heavy oil will not be heated sufficiently to reduce its viscosity which allows it to flow. This can result in a significant loss of thermal energy.

One other observation from the structural position of the bottom water is that the heavy-oil – water fluid contact is not flat. Van Hulst made this observation and suggested that it was related to structural movement combined with the inability of the

high viscosity oil to move and re-establish a flat fluid contact. The structural movement can be explained with the differential dissolution of the Prairie Evaporite or differential compaction.

### **2.3 Core analysis**

Numerous core samples of the Waseca formation have been acquired during the drilling of the Pikes Peak field. These cores serve to provide small scale evaluation of the reservoir. A rock physics study was performed using core samples from the D2-6-50-23W3 well at Core Laboratories. Measurements of acoustic wave traveltimes were made through the core samples that simulated conditions in the Pikes Peak field. The measurements examined the effect of temperature on the compressional ( $V_p$ ) and shear ( $V_s$ ) velocities. The core was cut from the reservoir 19 years before this detailed analysis was done.

The core tests cannot fully replicate the conditions in the reservoir. Once the core and heavy oil has been exposed to atmospheric conditions (or above the bubble point), it is considered to be 'dead'. That is, any gas that may have been held in solution in the reservoir ('live' conditions) has had the chance to escape. Wang and Nur (1992) demonstrated that dissolved gases can significantly lower the compressional velocity.

Two core samples taken from different measured depths (493 m and 505 m MD) in the D2-6 wellbore were independently tested to measure the effect of temperature on  $V_p$  and  $V_s$ . The tests were performed at a constant pore pressure of 2 200 kPa and a confining pressure of 9 200 kPa to account for the fluid pressure gradient and overburden pressure.

Figure 2-13 is a plot of  $V_P$  and  $V_S$  versus temperature for the sample taken from 505 m MD. The chart shows that  $V_P$  decreases 21.1 percent over a temperature range of 22° C to 160° C. The decreasing velocity with increasing temperature is mainly caused by the increasing compressibility.  $V_S$  decreases 15.2 percent over the same temperature range. The corresponding  $V_P/V_S$  decreases 6.9 percent. The second sample, from 493 m MD, had a  $V_P/V_S$  decrease of 8.4 percent under the same testing conditions.

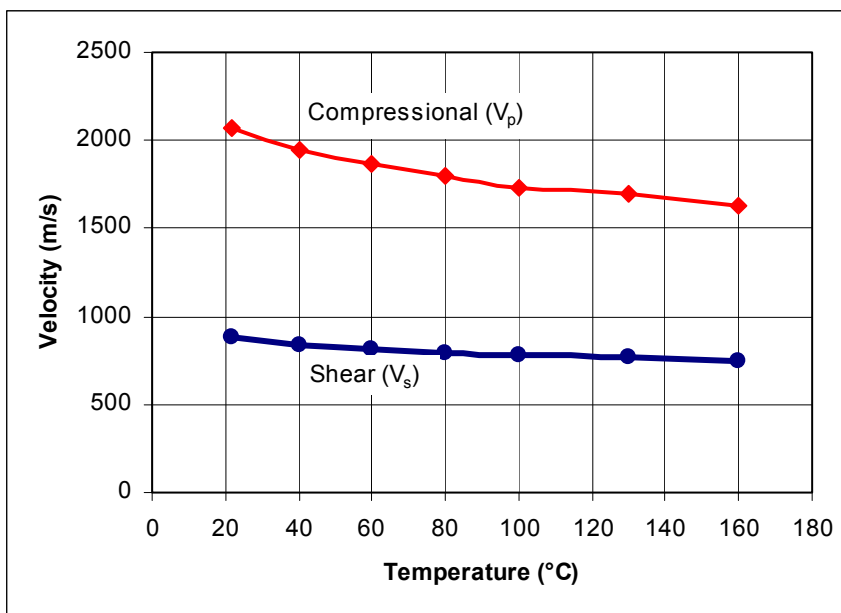


Figure 2-13: Effect of temperature on  $V_P$  and  $V_S$  from core samples.

The results of the effect of temperature on heavy-oil core velocities are consistent with laboratory tests performed by Wang and Nur (1988) and Eastwood (1993) for similar unconsolidated or weakly consolidated sandstone samples. Wang and Nur (1992) compared the velocities of heavy and light hydrocarbons. They suggested that the

melting of asphalteens and waxes commonly associated with heavy oils causes a faster velocity decrease in heavy hydrocarbons than in lighter varieties.

Another test was done to attempt to simulate the steam-flood conditions in the Waseca reservoir. A sample, also from 505 m MD, was loaded in a core holder and had a confining pressure of 9 200 kPa applied to it. The core holder was connected to a steam generator and heated in an oven to 160 °C. The sample was steam-flooded until no oil was produced. At a pore pressure of 2 200 kPa and the 9 200 kPa confining pressure and 160 °C temperature the compressional and shear velocities were measured. The results are summarized in Table 2-1 comparing this sample after steam reservoir conditions with a sample at original reservoir conditions.  $V_P/V_S$  dropped 16.1 percent. Dean Stark analysis (a laboratory extraction of oil and water from core samples using toluene as a solvent) showed that the sample had an original oil saturation of 78.5 percent. Post steam flood the sample had an oil saturation of 37.1 percent.

Table 2-1: Comparison of core analysis at reservoir condition before and after steam-flood.

Sample condition	Temperature °C	Pore Pressure kPa	Confining Pressure kPa	$V_P$ m/s	$V_S$ m/s	$V_P/V_S$
Original	22	2 200	9 200	2065	880	2.35
Steam-flood	160	2 200	9 200	1076	547	1.97

The results of the core analysis were encouraging to proceed with the interpretation analysis presented in Chapter 5. The effect of increased temperature and steam in the

reservoir is expected to reduce  $V_p/V_s$ . The effect of gas saturation could not be tested but is another condition in the reservoir that may contribute to changes in  $V_p/V_s$ .

## 2.4 Temperature Data

To help reservoir engineers understand the movement of steam and heat in the reservoir, temperature logs are acquired. Husky provided a couple samples of temperature log data that show elevated reservoir temperatures in new wells away from the current steam injection/production area. For example, the wells 5A2-6 and 6A2-6 were drilled into heated reservoir. The 5A2-6 well was drilled in March 1998, 95 meters away from a steam injection well, 2A2-6. The temperature log was only successfully run to the top of the Waseca interval but a temperature reading of 38°C was recorded. This suggests an elevated temperature above the original reservoir temperature of 18°C.

The 6A2-6 well (Figure 2-14) was also drilled in March 1998, 65 meters from the same injector well 2A2-6. This temperature log was run over the entire reservoir interval and encountered temperatures greater than 150°C. The 2A2-6 well had been continuously injecting steam into the reservoir since August 1992, over five and half years before the 5A2-6 or 6A2-6 well were drilled. There were no other wells in the vicinity that had been injecting steam into the reservoir during that time period. This demonstrates how the steam and heat had moved through the Waseca reservoir away from the injectors.

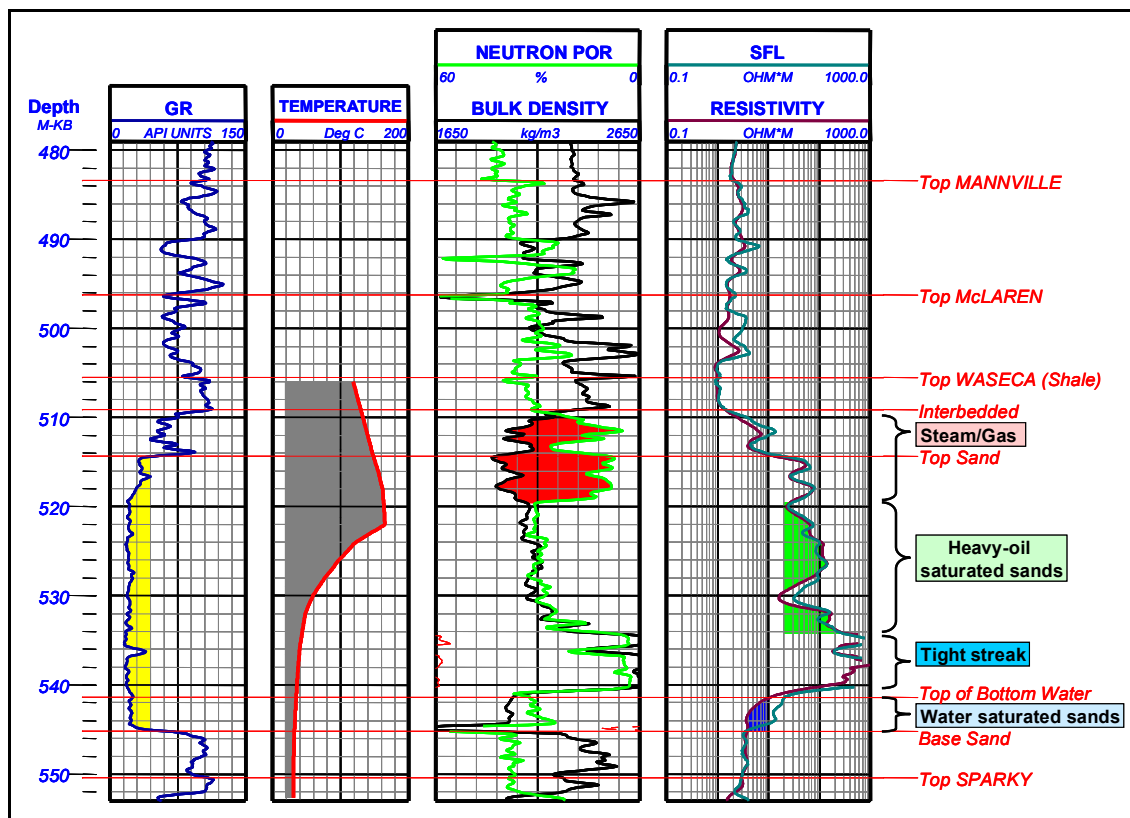


Figure 2-14: 6A2-6 temperature log over the Waseca interval and other corresponding logs.

The results of these two wells cannot be used directly in the time-lapse analysis of the seismic data because the data was not acquired at the time of the seismic shoots. The data does provided evidence of the distance the steam and heat fronts move through the reservoir. The logs from 6A2-6 also indicate how a gas has come out of solution and collected at the top of the Waseca interval. The cross-over of the neutron and density logs indicates gas. When the heavy oil is heated this draws the gas out of solution. In the reservoir simulation work by Zou et al. (2003) at Pikes Peak, seismic responses are significantly affect by this gas coming out of solution and increasing the gas saturation at the top of the reservoir interval.

## Chapter 3

### Impedance Inversion

#### 3.1 Inversion Theory

The seismic reflectivity data were used to invert for acoustical impedance. Acoustic Impedance (AI) is different from reflectivity data because it is an interval property rather than an interface property. Consider a simple two layer model (Figure 3-1) which has acoustic impedance values of  $Z_i$  and  $Z_{i+1}$ , where  $Z_i = \rho_i * V_i$ , the product of density ( $\rho_i$ ) and velocity ( $V_i$ ), for a given interval,  $i$ .

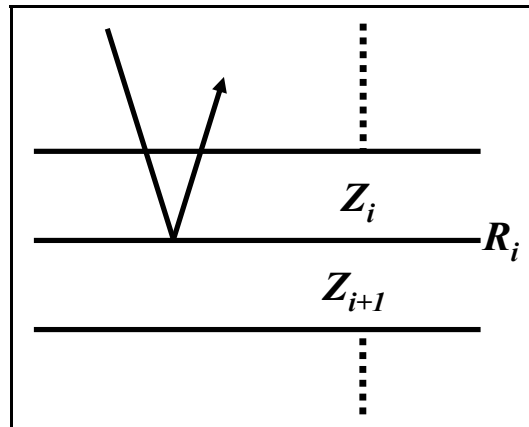


Figure 3-1: Simple two layer impedance model (McQuillin et al. 1979).

Equation 3-1 (McQuillin et al., 1979) derives the reflection coefficient,  $R_i$ , at an interface.

$$R_i = \frac{Z_{i+1} - Z_i}{Z_{i+1} + Z_i} \quad (3-1)$$

Rearranging Equation 3-1 to solve for  $Z_{i+1}$  gives Equation 3-2.

$$Z_{i+1} = \frac{Z_i(1 + R_i)}{1 - R_i} \quad (3-2)$$

Given a reflectivity sequence such as a seismic trace and an initial acoustic impedance value,  $Z_i$  the trace can be inverted to give acoustic impedance with time or depth as Equation 3-2 is used iteratively. This method is described in a classic paper by Lindseth (1979). In this study a type of ‘trace based’ inversion is performed where information from non-seismic data sources constrains the results. AI has the effects of wavelet sidelobe energy and tuning removed. This improves the interpretation of boundaries and allows evaluation of the internal rock properties (Buxton Latimer et al., 2000).

Lindseth also showed that a simple sonic log can be considered as the sum of a smooth velocity function (0 - 5 Hz) and a detailed velocity function (6 - 250 Hz) which mimics a seismic trace in character (Figure 3-2). In a similar way this analysis can be used to demonstrate how seismic data, which is band limited, lacks the DC and low frequency information. In most geological cases impedance increases with depth but if a seismic trace were inverted on its own the DC and low frequency information would be absent. In order to capture this missing impedance information another source such as sonic and density logs are needed. By merging DC and low frequency information from impedance logs with a band-limited impedance section the spectrum can be optimized.

Injecting steam in the reservoir formation reduces the AI due to the lowering of seismic velocities as observed with the core analysis. A consequence is an increased traveltime in the reservoir.

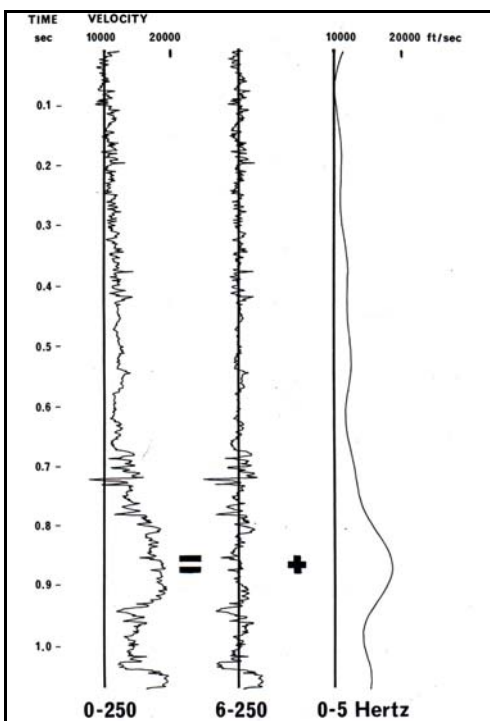


Figure 3-2: Composition of a sonic log (Lindseth 1979).

### 3.2 Inversion Process Overview

The key inputs to the Jason inversion process are the impedance logs in time, the seismic data and interpreted horizons. The horizon and impedance logs are used to create an ‘earth model’, which in turn is used to constrain the inversion process (Figure 3-3a). After the inversion of the seismic traces, the low-frequency AI from the earth model (Figure 3.3b) and band-limited AI (Figure 3.3c) inverted from the seismic are merged to give a full impedance section (Figure 3.3d). The objective in this study was to observe the differences in AI on the time-lapse data set. It was not within the scope of this study to continue on to the net pay and porosity prediction. Throughout the inversion process

there are several quality control (QC) checks to ensure that appropriate parameters are chosen and that the process is being followed correctly.

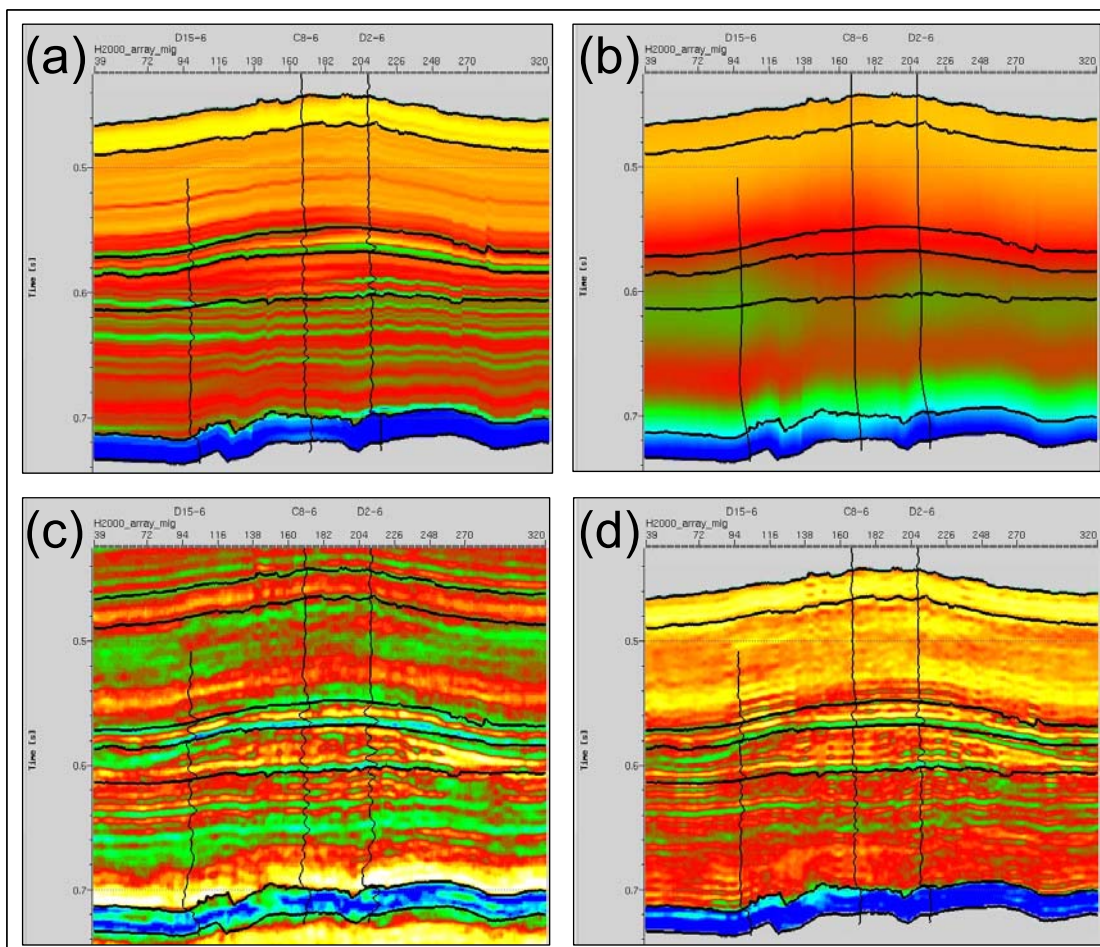


Figure 3-3: Summary of the H2000 inversion process. (a) Earth model built using impedance well log data, (b) Low-pass filter of earth model (from well log data), (c) Band-limited inversion (from seismic data), and (d) Result of merged low-pass filtered well data and band limited inversion.

Note the impedance logs shown are filtered to the same bandwidth as the data in each case.

An important aspect of the inversion process is the choice of wavelet. Because of the different frequency content of the two time-lapse lines, two different wavelets for the surveys were required. Wavelets were estimated using a deterministic model driven approach that included the reflectivity of the wells logs. Wavelet estimation was an

iterative process that improved as the synthetic tie and wavelet improved. Interpreted horizons and impedance logs were used to create an earth model, which in turn was used to spatially constrain the inversion process. Constraints were also set on a range of physically realizable AI values. After the sparse spike inversion of the seismic traces, the low frequency AI from the earth model and band-limited AI from the seismic inversion were merged to give a full AI section

### **3.2.1 Synthetic Tie and Interpretation**

In this study the log curves from three wells (D15-06, C08-06 and D02-06) were used. These wells were chosen because they had sonic and density logs run over the Waseca interval and they were relatively close to the lines. They ranged from 50-110 m perpendicularly from the two lines.

Sonic and density log pairs extending down into the Devonian were preferred so that the zone of interest is in the middle of the analysis window and the large impedance contrast at the PreCretaceous Unconformity could be included. Composite logs were built by borrowing logs in the lower section from nearby wells. The assumption is that the geology or impedance of the lower sections does not vary dramatically in the extent of the field. Significant horizon markers were interpreted on the logs.

The two migrated sections and the sonic and density curves from the three key wells were loaded into Jason Geoscience Workbench for the inversion process.

With the well logs loaded into Jason synthetic forward models were created and tied to the two seismic sections. The most important aspect of the synthetic tie (and,

furthermore, the entire inversion process) is the choice of wavelet. A deterministic model driven approach to wavelet estimation was used in the Jason software package. This approach uses the reflectivity information from the well logs and seeks to design a wavelet to minimize the differences in the amplitude and phase between a synthetic at the wells and the nearest traces on the seismic line. No prior assumptions of amplitude or phase spectra are required and the wavelet does not contain noise from the seismic data. Because of the different frequency content of the two time-lapse lines two different wavelets were required. Wavelet estimation was an iterative process that improved as the tie and wavelet improved. With a reliable synthetic tie the following horizons were then interpreted across the seismic sections (see Figure 3-4): Base of Fish Scales ('BFS'); Mannville top ('MNVL'); Waseca top; Sparky top; and, the PreCretaceous Unconformity/Devonian top ('PCU').

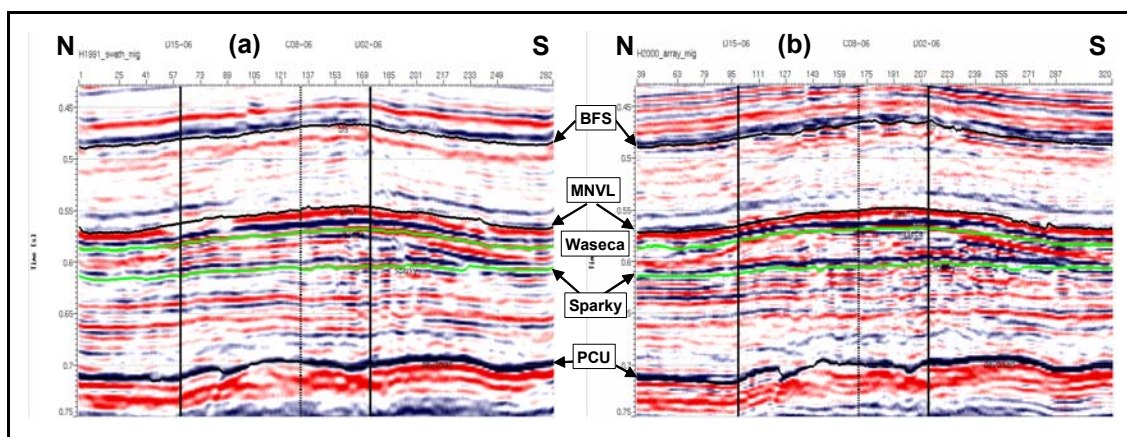


Figure 3-4: Interpreted (a) H1991 and (b) H2000 with key horizons used for earth model building.

### **3.2.2 Earth Model**

A geologic framework was built using the interpreted time horizons for each line. In this Western Canada Plains case study the model is quite simple and relatively flat but in areas with significant folding and faulting, the framework can be complex. The expected stratigraphic relationships at the horizon boundaries such as truncation, downlap, toplap or parallel to top and base were specified in the geologic model. An example would be the PreCretaceous Unconformity which truncates the geology below it but has clastic sequences downlapping on to it from above.

The earth model framework acts as a vertical constraint on the inversion. In the earth model generation process the impedance values from the three wells are extrapolated across the model bounded by the horizons and stratigraphic relationships (Figure 3.3a). Since more than one well tied to the section the impedance values across the earth model section were weighted to the values at the closest well using an inverse-distance extrapolation or interpolation method.

### **3.2.3 Inversion**

The Jason module used for these inversions is called Constrained Sparse Spike Inversion (CSSI). This algorithm minimizes the difference (or residual) between seismic trace data and the earth model convolved with a given wavelet. The term 'sparse spike' refers to the goal of the algorithm to create the simplest acoustic impedance model, or the fewest reflection coefficients, while minimizing the residuals. A trade-off is required.

For this process a priori knowledge of the geology and well logs has been used to constrain the initial model.

Before running the inversion the constraints on the impedance values for a given interval need to be defined (Figure 3-5). The range of values limits the number of possible acoustic impedance solutions. High and low spikes of impedance are seen on the logs. These spikes are caused by calcite-cemented tight steaks and coals. A trend line is fit to the impedance log to smooth through these spikes and provide a baseline for the inversion result. With the log high-cut filtered down to 150 Hz (the upper limit of the reflection data) many of these spikes disappear. It was safe to assume that the seismic would not be able to resolve them and, therefore, they would not factor into the inversion result.

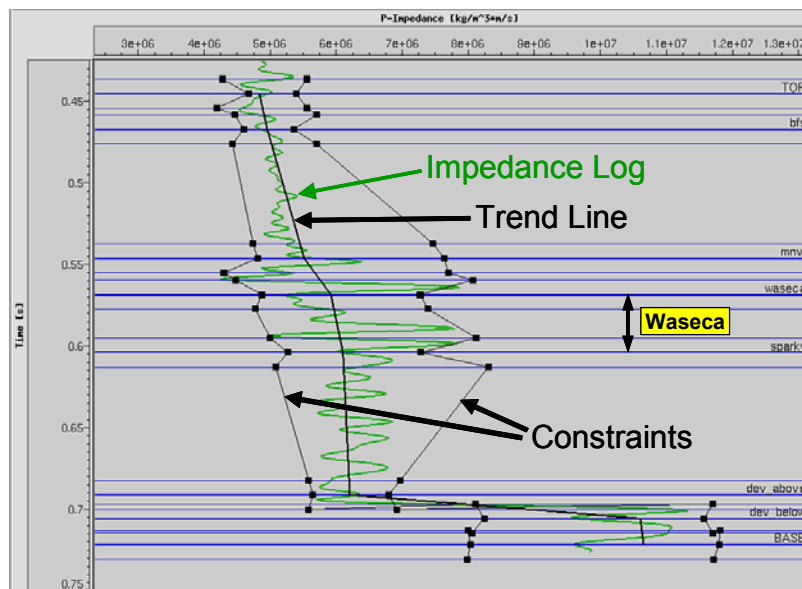


Figure 3-5: Constraint editor for CSSI. The trend and constraint lines set boundaries on the solution space of the inversion.

The inversion was not forced to match the wells. It only requires the solution to lie within the prescribed constraints. Within the CSSI process there were various QC tools to observe the difference or residual between the real reflectivity data and modelled reflectivity. The goal was to minimize the residual. The solution could not be perfect or unique. Noise in the data and an incomplete wavelet are the main contributors to differences. With the optimal inversion parameters selected the CSSI was run. The next step was to merge this data with low frequency information from the well data.

#### **3.2.4 Trace Merge**

The result of the inversion is band limited. The values of impedance were positive or negative. To obtain the optimal spectrum that observes increasing impedance with depth, filters that act on the earth model and CSSI result are designed in the frequency domain. Figure 3-6 shows how the filters were designed for the H2000 inversion. A low-pass filter, preserving 0-10 Hz applied to the earth model results in smoothly increasing impedance sections in time. A complementary band-limited filter, preserving 10-110 Hz applied to the CSSI result provides an impedance section similar in appearance to reflection data because there is no bias or DC component in the data.

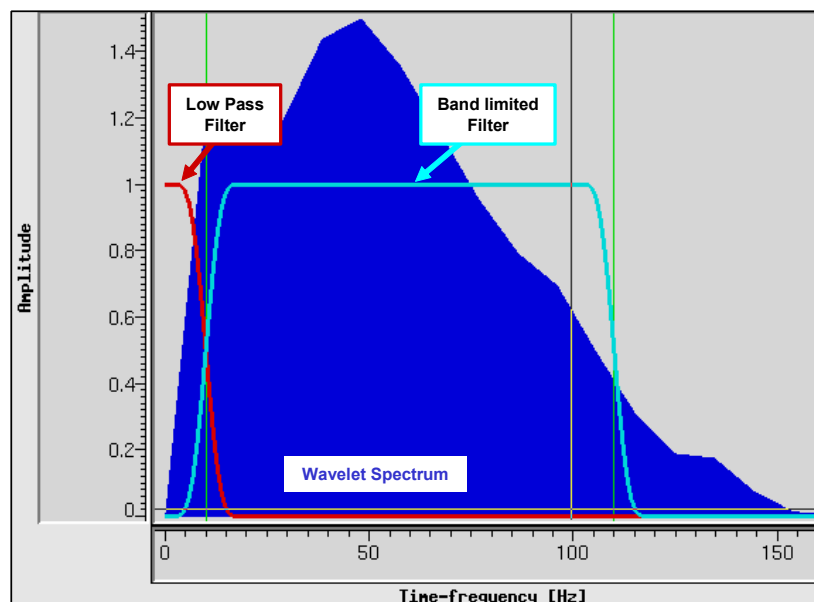


Figure 3-6: Trace merge filter design. The low-pass filter was applied to the impedance well log interpolated earth model. The band-limited filter was applied to the inversion result. The spectrum of the wavelet used in the inversion process is shown in the background.

The final act involves merging filtered sections to give the final impedance sections in Figures 3-7 and 3-8 for H1991 and H2000 respectively. Direct comparison of the two sections in the reservoir (Waseca-Sparky) zone can be made because the sections are impedance sections rather than reflectivity sections which were dependent on the (removed) wavelet. The high-cut filtered impedance logs from the three wells are overlain on the full impedance sections for direct comparison. The success and quality of the inversion can be judged by this comparison. The Jason inversion does not force the inversion to match the wells. It only requires the solution to lie within the prescribed constraints. There is very good qualitative agreement. On both sections at the PCU (700 msec) there is a sharp increase in impedance as the lithology changes from the overlying clastics to carbonate.

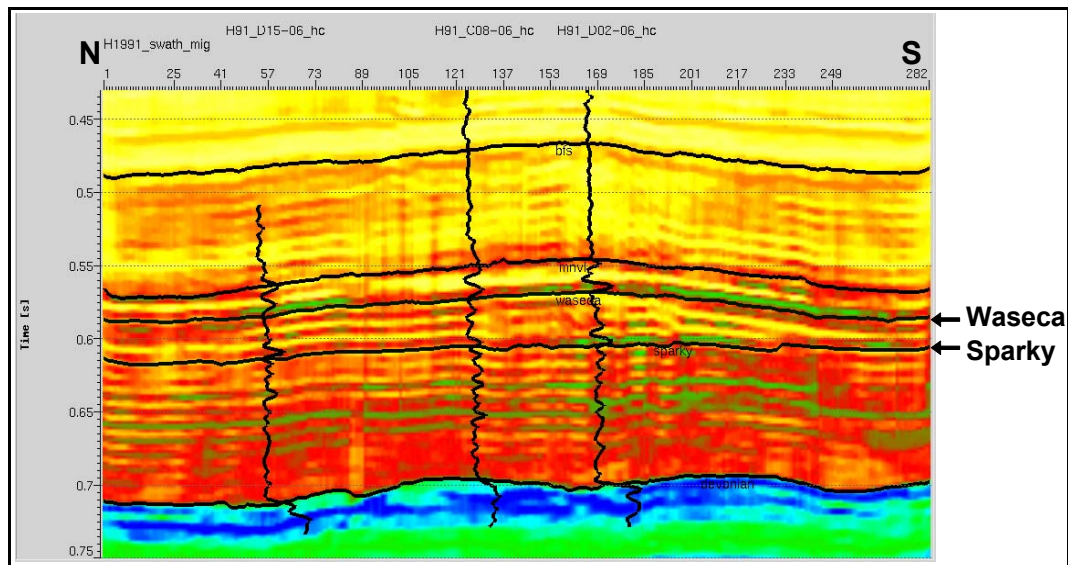


Figure 3-7: Full acoustic impedance section of H1991 with three impedance logs overlain.

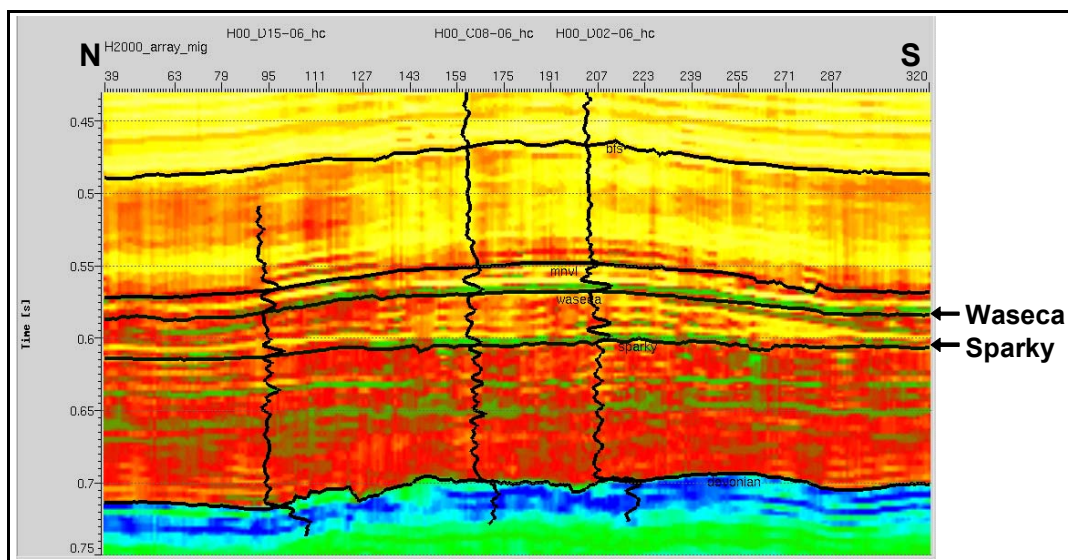


Figure 3-8: Full acoustic impedance section of H1991 with three impedance logs overlain.

## Chapter 4

### Time-lapse Analysis

#### 4.1 Introduction

The east side of the Pikes Peak field was the ideal location to test and evaluate time-lapse analysis. The H1991 seismic data covered the northeast portion of the field that in 1991 had not been developed. By 2000 this area of the field had a number of new development wells drilled into it. Figure 4-1 shows the development of the field in (a) February 1991 and (b) March 2000. The numbers of wells that are located adjacent to the time-lapse seismic surveys nearly doubled.

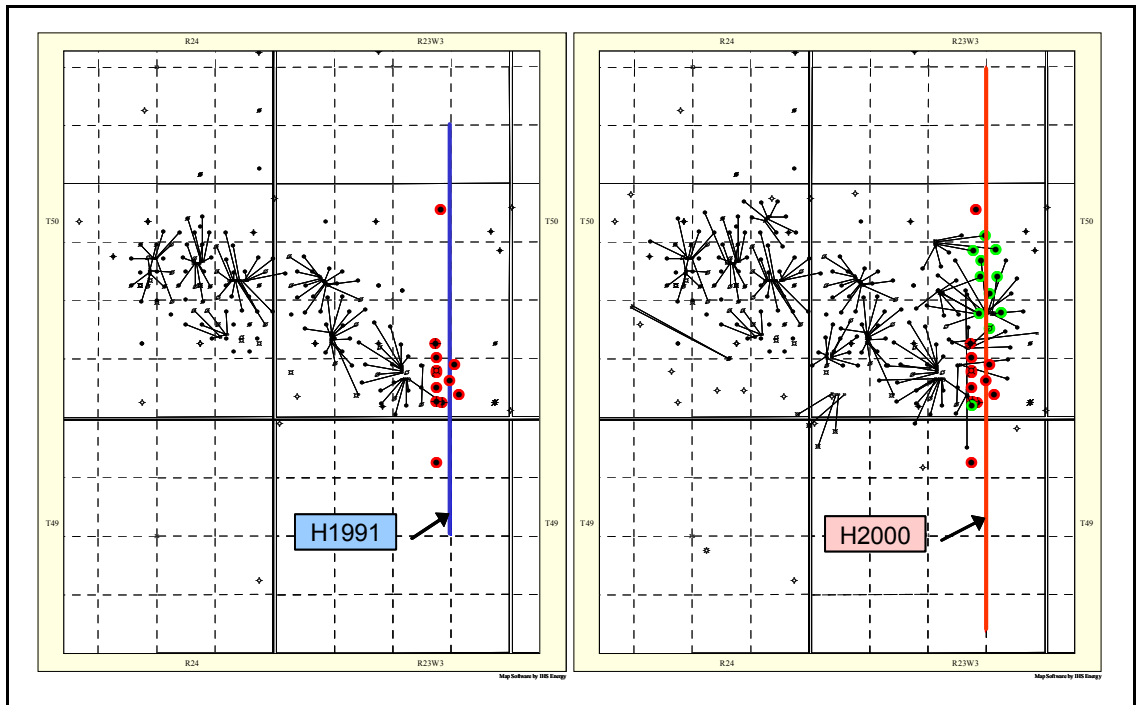


Figure 4-1: Maps of the Pikes Peak field in (a) February 1991 and (b) March 2000. Wells adjacent to the time-lapse seismic surveys are highlighted. The red wells were drilled prior to February 1991 and the green wells were drilled between February 1991 and March 2000.

The most northern well adjacent to the seismic lines as shown in Figure 4-1, D15-6, was drilled prior to 1991 but has not undergone any injection or production.

The wells adjacent to the time-lapse lines that were active in 1991 had undergone various phases of steam injection and heavy-oil production prior to the H1991 acquisition. This southern portion of the line would be considered 'altered' reservoir. The remainder of the line to the north acts as true base survey for the H2000 seismic line. The changes that can be observed on the H2000 data are complex. On the southern portion of the line, more altered reservoir can be compared to the 1991 altered state. On the northern portion of the line, reservoir that as has be altered between 1991 and 2000 can be compared to unaltered or original reservoir conditions.

Since Husky Energy began operations at Pikes Peak they have not maintained the original reservoir pressure (3 350 kPa) as they have recovered the heavy oil. Husky engineers estimated that in 1991 and 2000 the background or virgin reservoir pressure would be 2 200 kPa on the eastern side of the field. Pressure changes may contribute to time-lapse differences.

Many of the wells have undergone several status changes over time. Table 4-1 shows the predicted steam zone radii and time since steam had been injected into six wells adjacent to H1991 and H2000. These wells were chosen because the Husky engineers had estimated that the steam zone radius for these wells was sufficient to project on to the seismic lines of investigation (Figure 4-2). For example, the well 3B1-6 was originally drilled in 1982 and has had six status changes, alternating between steam injector and

heavy-oil and water producer. During the H1991 acquisition it was a steam injector. In March 2000 it was a producer and it had been 14 months prior to that since it was an injector. Large swings in the reservoir pressure occur at these well locations as they change status. In January 1991 the estimated reservoir pressure at 3B1-6 was 4500 kPa – double the virgin reservoir pressure of 2 200 kPa. In November 1999 (four months prior to the H2000 survey) the estimated reservoir pressure at 3B1-6 was 1 200 kPa. The dates for the pressure readings do not correspond exactly with the seismic acquisitions. The pressure variations in this one well demonstrate how steam-assisted recovery methods can affect the dynamics of a reservoir. Zou et al. (2003) provides the initial results of a comprehensive reservoir simulation in an area of the Pikes Peak field that includes the wells adjacent to the time-lapse seismic data.

Table 4-1: Predicted steam zone radii and time (in months) since steam was injected into key wells adjacent to H1991 and H2000.

Well	Predicted steam zone radius (m)		Number of Months since last steam injection	
	Feb. 1991	March 2000	Feb. 1991	March 2000
<b>3B1-6</b>	6.0	44.0	<1	14
<b>1D2-6</b>	22.3	31.5	38	25
<b>3C1-6</b>	19.8	44.2	67	89
<b>3B8-6</b>	not drilled	25.4	not drilled	0 (concurrent)
<b>2B9-6</b>	not drilled	37.2	not drilled	26
<b>1D10-6</b>	not drilled	29.8	not drilled	12

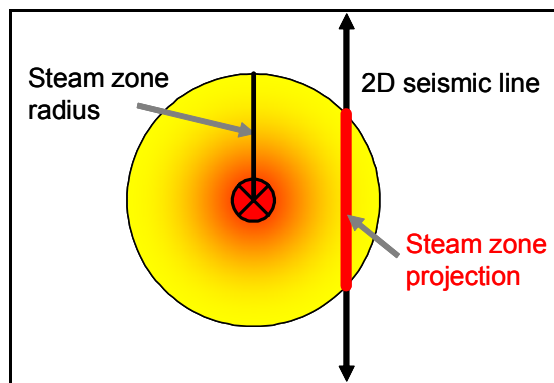


Figure 4-2: Schematic to illustrate how the steam zone projects on to the 2D seismic lines.

Three analysis techniques were used to see how the seismic response was affected by changes to the Waseca reservoir interval between 1991 and 2000. The first two methods involve the differencing of reflectivity and impedance sections. The third method is interpretation based and observes the changes in seismic traveltimes through the Waseca.

#### 4.2 Reflectivity Differencing

The time-lapse seismic lines, H1991 (Figure 1-6) and H2000 (Figure 1-7), were loaded into Hampson-Russell Pro4D to perform the reflectivity differencing. Prior to subtraction of the reflectivity sections they needed to be compared and calibrated to adjust for static, amplitude and phase differences. It was critical that the time window for the calibration was above the zone of interest where the recorded seismic signal was not affected by the reservoir zone. Trace-by-trace comparisons provided the best results.

The reflectivity data difference, Figure 4-3, had the clearest difference section when a wavelet-shaping filter was applied to the H2000 line to match it to the H1991 line. Figure 4-3 also shows the bottom-hole location of the six wells (from Table 4-1) in close

proximity to the time-lapse lines that had had cyclical steam injection and production from them between 1991 and 2000. The most significant differences in the section are seen below the reservoir zone in the area of these production and injection wells. An increase in travelttime through the reservoir zone on the H2000 data was caused by the presence of injected steam and heat in the reservoir. This time delay did not allow the signal of deeper events to cancel. Therefore, all reflections from reflectors below the heated reservoir zone are affected. The differences are small at D15-06 location, the well furthest to the north (left), where no steam injection or production has occurred. The seismic modelling results of Zou et al. (2002) generally agree with these real data results.

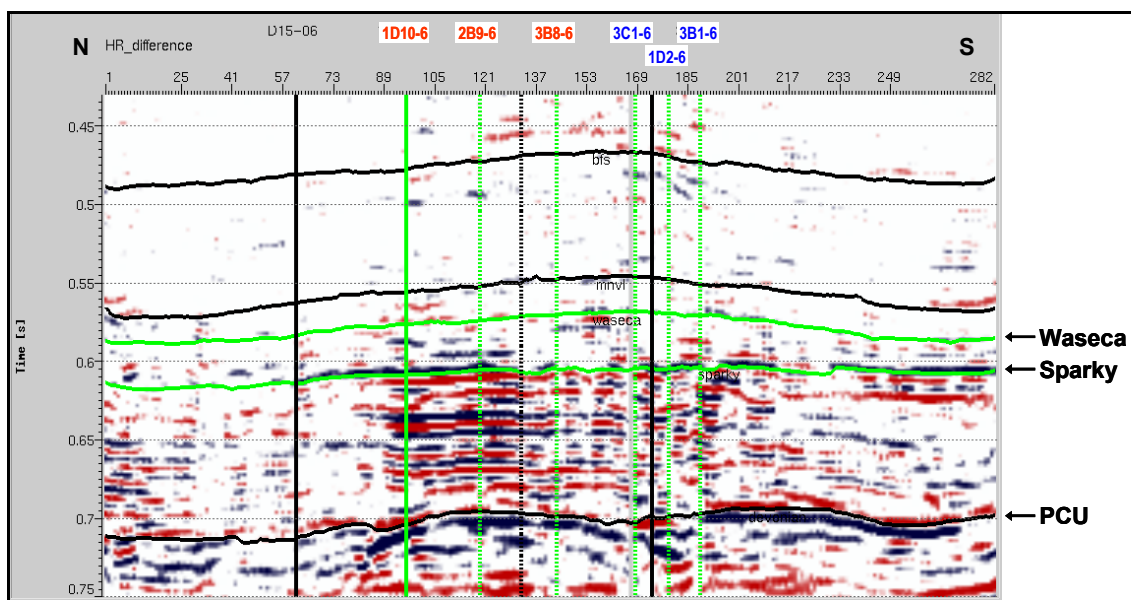


Figure 4-3: Seismic reflectivity difference section.

Some differences occur in the section where they were not anticipated. For example, the bright difference at the PCU south of the wells may be caused by a difference in the processing velocities of the time-lapse lines. Another cause of poor signal cancellation

outside of the developed area of the field may be the fold differences between the surveys, especially at the ends of the H1991 line (1 km shorter than H2000).

### 4.3 Impedance Section Differencing

Following the acoustic impedance inversions discussed in Chapter 3 the AI sections were brought into Hampson-Russell's Pro4D module. Before the subtraction of the impedance sections the H2000 line required a band-pass filter, wavelet shaping and time and phase matching to calibrate it to the H1991 line.

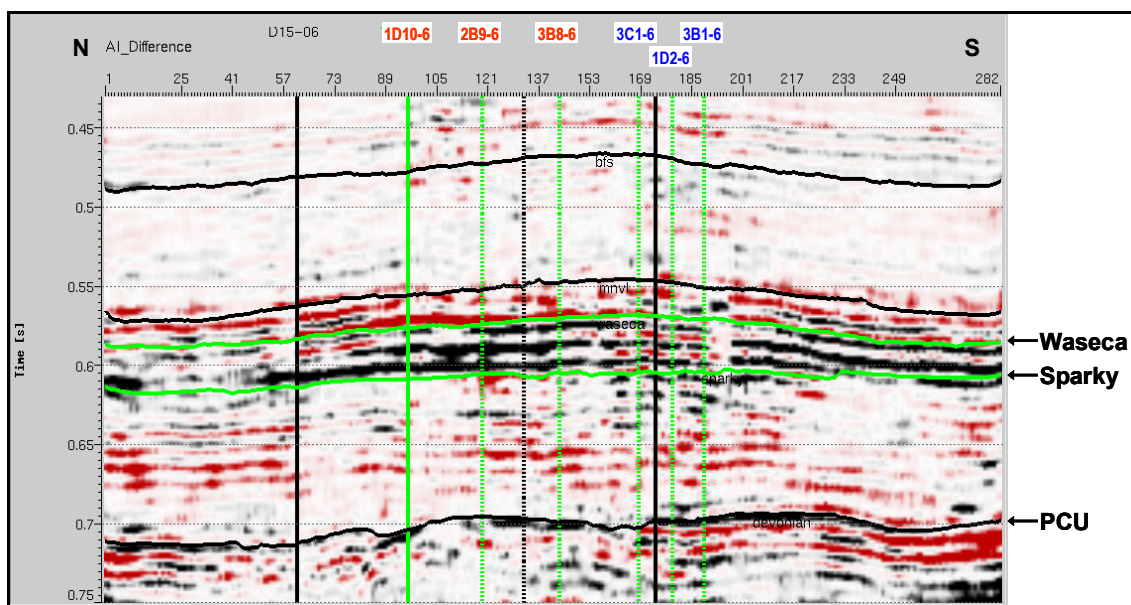


Figure 4-4: Acoustic impedance difference section.

The acoustic impedance difference is shown in Figure 4-4 with the six wells from Table 4-1 annotated. The most significant differences are seen in the zone of interest where there is a lower impedance zone. Unlike the results at D15-06 on the reflectivity difference, the lower impedance zone appears to reach this well and extend further to the

south than anticipated. One explanation of this anomalous decrease in impedance outside of the well control may be changes in reservoir pressure. There is no appropriate well data to directly confirm the location and magnitude of the pressure changes. However, pressure changes are anticipated as the Husky operations allow the overall reservoir pressure to drop with ongoing production. The greatest differences are seen in the reservoir interval around the production and injection wells but they are not exclusively lower impedance values. Has some post-steam cementation occurred to cause higher impedance values? These 2-D seismic data alone cannot answer these questions.

#### **4.4 Isochron analysis**

The isochron or delay-time analysis method used the interpretation of the Waseca interval for the two vintages of lines. The H1991 and H2000 geophone array data were used. The use of traveltimes eliminates any concern for static differences in the post stack data. Moreover, the traveltimes picking of seismic data is generally a very robust method.

The bandwidth differences meant that there was greater resolution for picking events on the H2000 stack as compared to the H1991 stack. As a result, slight differences caused by tuning in the interpretation were anticipated. The interpretation of the Waseca-Sparky interval on both versions is shown in Figures 1-6 and 1-7.

At each CDP the ratio of the H2000 to H1991 Waseca interval traveltimes were calculated and plotted in Figure 4-5. With the injection of steam and heat in the reservoir in the time between the two surveys a drop in P-wave velocity is expected. This decrease

translates into an increase in the H2000/H1991 isochron ratio. If there had been no changes in the reservoir between February 1991 and March 2000, the ratio would be unity.

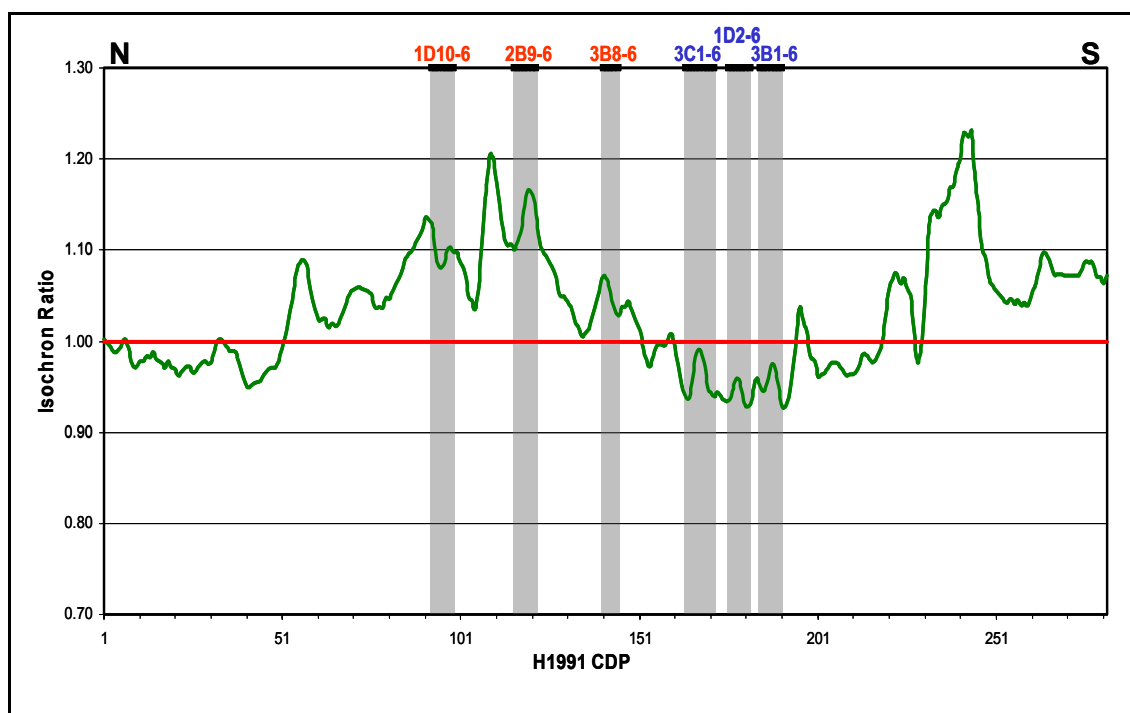


Figure 4-5: H2000/H1991 ratio of Waseca interval traveltimes for P-wave arrivals.

The estimated position and width of the steam zone from injection and production data were projected onto Figure 4-5 from six wellbores near the line (see Table 4-1). The three wells on the left (1D10-6, 2B9-6 and 3B8-6) were drilled during the time period between the two surveys. The ratio rises above unity in this section of the line. Conversely, the ratio drops below unity along the portion of the line where three older producers (3C1-6, 1D2-6 and 3B1-6) were more active in 1991 than in 2000. More heat and steam was present in this portion of the reservoir in 1991 and are responsible for the

ratio reversal. The width of the anomalies suggests that the compressional velocity is showing sensitivity to more than just the steam-zone radius around the wellbores. The total area of the heated reservoir also affects  $V_p$ .

## Chapter 5

### Multicomponent Analysis

#### 5.1 Introduction

As described in Chapter 2.3, the addition of steam into core from the Pikes Peak reservoir has the effect of decreasing both  $V_P$  and  $V_S$  but  $V_P$  decreases at a greater rate. Therefore, it is anticipated that steam injection into a sand unit would cause a decrease in  $V_P/V_S$ . This characteristic of  $V_P/V_S$  can be effectively utilized for steam-front monitoring where multicomponent data is available.

A method to derive  $V_P/V_S$  can be achieved by expressing the thickness of a depth interval in terms of P-wave and S-wave traveltimes. For converted-wave data to be generated there needs to be some offset (no normal incidence). The converted-wave (P-S) data is processed such that the offset data normal moveout corrected and stacked into an equivalent normal offset seismic section. Figure 5-1 illustrates how the compressional and converted-wave data travels through an interval of equivalent thickness.

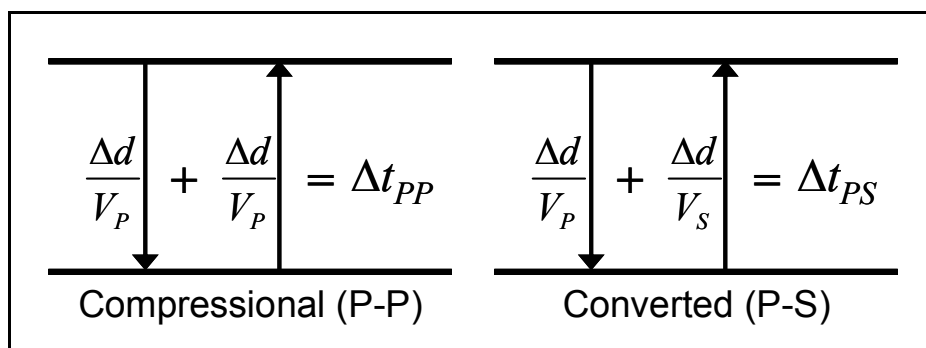


Figure 5-1: Traveltimes through a constant thickness interval for compressional and converted waves.

A compressional (P-P) wave travels twice, down and up, through an interval,  $\Delta d$ , at the P-wave velocity,  $V_P$ . The interval two-way traveltime,  $\Delta t_{PP}$ , can be expressed as in Equation 5-1.

$$\Delta t_{PP} = \frac{2\Delta d}{V_P} \quad 5-1$$

Similarly, a converted (P-S) wave travels down through the same interval,  $\Delta d$ , at the P-wave velocity,  $V_P$ , and after mode conversion travels back up through the same interval as an S-wave with velocity  $V_S$ . The converted-wave interval two-way traveltime,  $\Delta t_{PS}$ , can be expressed as the sum of the two directions of travel given in Equation 4.

$$\Delta t_{PS} = \frac{\Delta d}{V_P} + \frac{\Delta d}{V_S} \quad 5-2$$

Solving Equations 5-1 and 5-2 for  $\Delta d$  gives Equations 5-3 and 5-4, respectively.

$$\Delta d = \frac{\Delta t_{PP} V_P}{2} \quad 5-3$$

$$\Delta d = \Delta t_{PS} \left( \frac{V_S V_P}{V_P + V_S} \right) \quad 5-4$$

With both equations set equal to  $\Delta d$  they can be combined into Equation 5-5a.

$$\frac{\Delta t_{PP} V_P}{2} = \Delta t_{PS} \left( \frac{V_S V_P}{V_P + V_S} \right) \quad 5-5a$$

Simplifying and rearranging gives Equations 5-5b, 5-5c and 5-5d.

$$\Delta t_{PP} = 2\Delta t_{PS} \left( \frac{V_S}{V_P + V_S} \right) \quad 5-5b$$

$$\frac{V_P + V_S}{V_S} = \frac{2\Delta t_{PS}}{\Delta t_{PP}} \quad 5-5c$$

$$\frac{V_P}{V_S} + 1 = \frac{2\Delta t_{PS}}{\Delta t_{PP}} \quad 5-5d$$

The final  $V_P/V_S$  equation can be expressed as Equation 5-6a, or as commonly published as shown in Equation 5-6b.

$$\frac{V_P}{V_S} = \frac{2\Delta t_{PS}}{\Delta t_{PP}} - 1 \quad 5-6a$$

$$\frac{V_P}{V_S} = \frac{2\Delta t_{PS} - \Delta t_{PP}}{\Delta t_{PP}} \quad 5-6b$$

The interval traveltimes  $V_P/V_S$  method is a relative measure of the average  $V_P/V_S$  over an interpreted interval.

Stewart et al. (1997) showed how the average  $V_P/V_S$  value of a set of layers is a weighted sum of interval velocity ratios. The more anomalous a  $V_P/V_S$  value is for a specific interval or the thicker the anomalous interval, the greater the influence on the average  $V_P/V_S$ . Miller (1996) suggested that the average  $V_P/V_S$  values of greater than 0.05 are measurable and should be able to resolve anomalous reservoir values.

The interval traveltimes  $V_P/V_S$  method assumes that there is no interpretation mismatch from the P-P and P-S seismic sections. An inevitable ‘picking ambiguity’ existed because it is difficult to ensure that the events picked are depth or geologically time equivalent. The bandwidth and resolution of the two sections is significantly different.

The values of  $V_p/V_s$  derived from Equation 5-6 provide valid apparent relative changes but not true  $V_p/V_s$  values (Margrave et al., 1998).

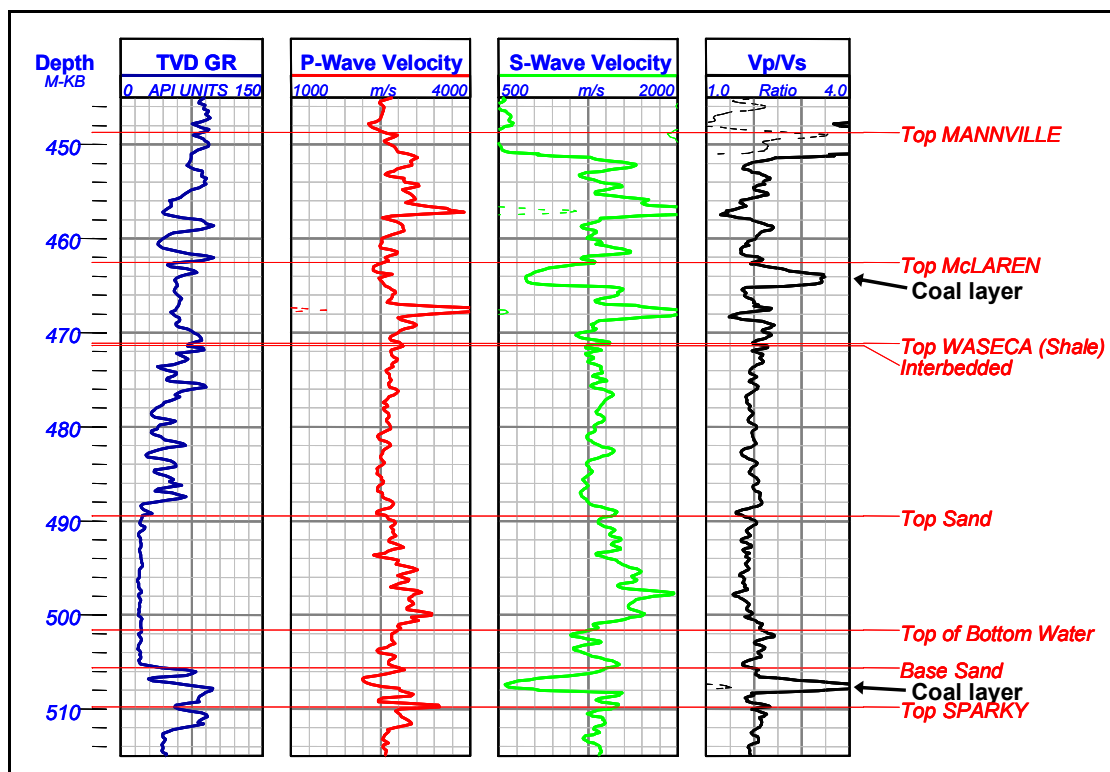


Figure 5-2: P- and S- wave velocity logs from the dipole sonic log at well 1A15-6.  $V_p/V_s$  was calculated directly from the velocity logs.

The P- and S- velocity logs from 1A15-6 are shown in Figure 5-2. These logs allowed for a simple calculation of  $V_p/V_s$  over the upper Mannville section including the Waseca. Near the Top Mannville and above  $V_p/V_s$  climbs well over a value of 4.0. Below the Top Mannville the values tends to range of 1.5 to 2.5.  $V_p/V_s$  increases significantly at two coal layers (marked on Figure 5-2) within the Mannville section. Within the Waseca interval, the interbedded zone has a slightly higher  $V_p/V_s$  value (average of 1.96) than the homogeneous sand (average 1.83). These values are perhaps the closest to the true  $V_p/V_s$

values for the Waseca. The isochron method averages  $V_P/V_S$  over a set of intervals. Another reason the two values are not likely to match is the method of acquisition. P- and S-waves measured in the surface seismic bandwidth (10 - 150 Hz) tend to have a slower velocity than those measured with open-hole logs (kHz) or in core (MHz). The differences are caused by dispersion, the variation of seismic velocities with frequency.

## 5.2 $V_P/V_S$ Interpretation

Similar to the time-lapse isochron analysis (Chapter 4.4),  $V_P/V_S$  analysis also is an interpretation-based travelttime method but only involves the multi-component data acquired in March 2000. No converted-wave data were collected in 1991. The vertical (P-P) and radial (P-S) components were used. For the P-P interpretation the vertical component of the 3C geophone was used. For the P-S interpretation the radial component was used. There was no appreciable signal on the transverse component. The radial converted-wave section required a synthetic that accounted for the wave conversion and the reduced bandwidth in the order of 8 – 40 Hz. A P-S synthetic with several offsets was created (see Figure 5-3) because there is no mode conversion at zero offset. The P- and S-wave sonic logs from 1A15-6 were used to create the P-S synthetic. The MATLAB code ‘synth’ was used to create the offset gather.

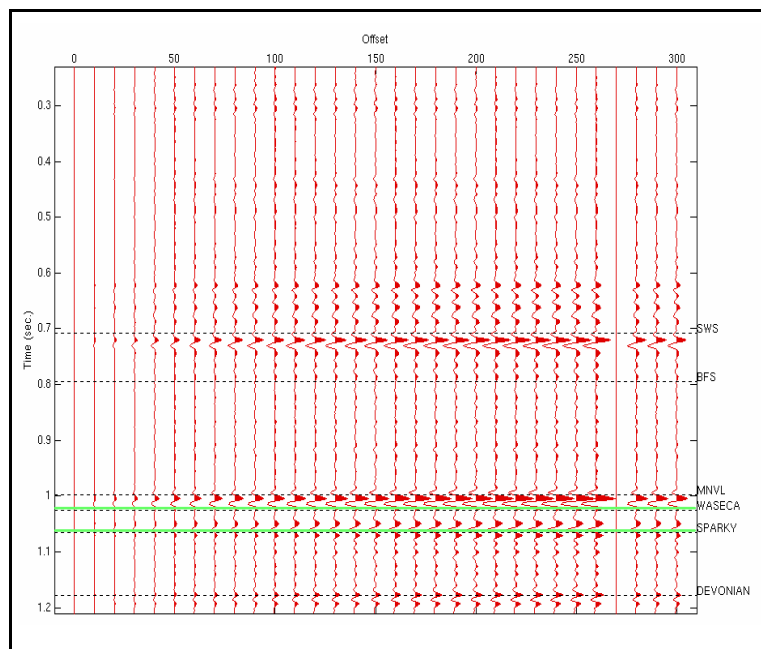


Figure 5-3: Converted P-S-wave synthetic created at 1A15-6.

Figure 5-4 shows the vertical component section for H2000, which is predominantly a P-P section. Figure 5-5 shows the radial component section, which is predominantly a P-S section. The two intervals, including the entire Waseca formation, on each section are considered to be geologically equivalent intervals based on the P-P and P-S synthetic ties. The Waseca-Sparky interval (same as Figures 1-5 and 1-6) and a larger Mannville–Lower Mannville interval are interpreted. The P-S section has a different time scale. The significantly lower bandwidth affects the resolution of picking horizons on the P-S section. The P-S stacked section also exhibits more noise. Fortunately, at 1A15-6 tie point the S/N is relatively higher around the zone of interest. Noise cones can be seen on the section to the south (right) of 1A15-6 in the area that coincides with active pump-

jacks (CDPs 323 - 459). The interpretation was forced through the noisier portions of the line.

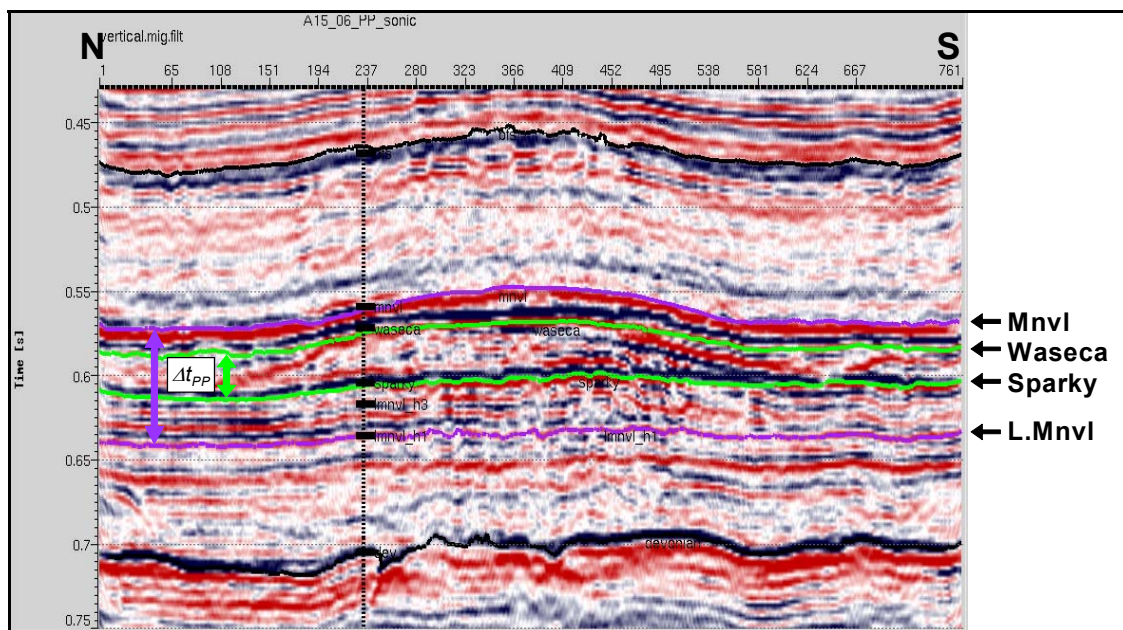


Figure 5-4: Interpreted H2000 P-P section (vertical component).

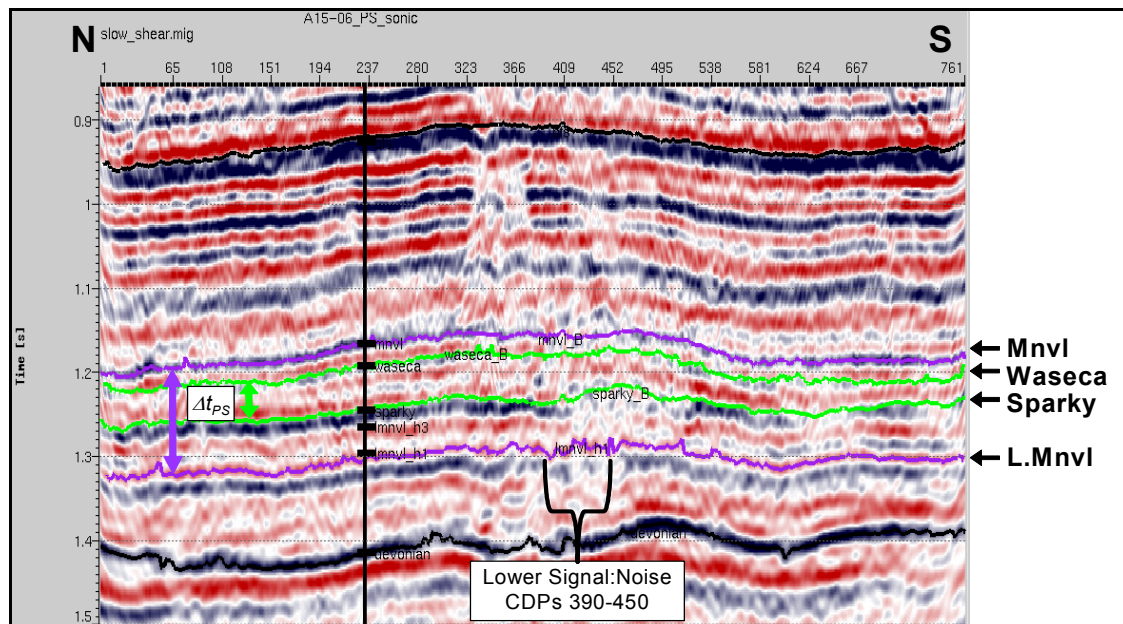


Figure 5-5: Interpreted H2000 P-S section (radial component). Note the different time scale.

### 5.3 $V_p/V_s$ Steam Front Analysis

The smaller window, Waseca-Sparky, was examined first and the  $V_p/V_s$  plot is shown in Figure 5-6. Noise dominates the ratio plot. There are relative drops in  $V_p/V_s$  which correlate with some of the wells but the large swings in  $V_p/V_s$  makes it difficult to confidently infer any steam effects.

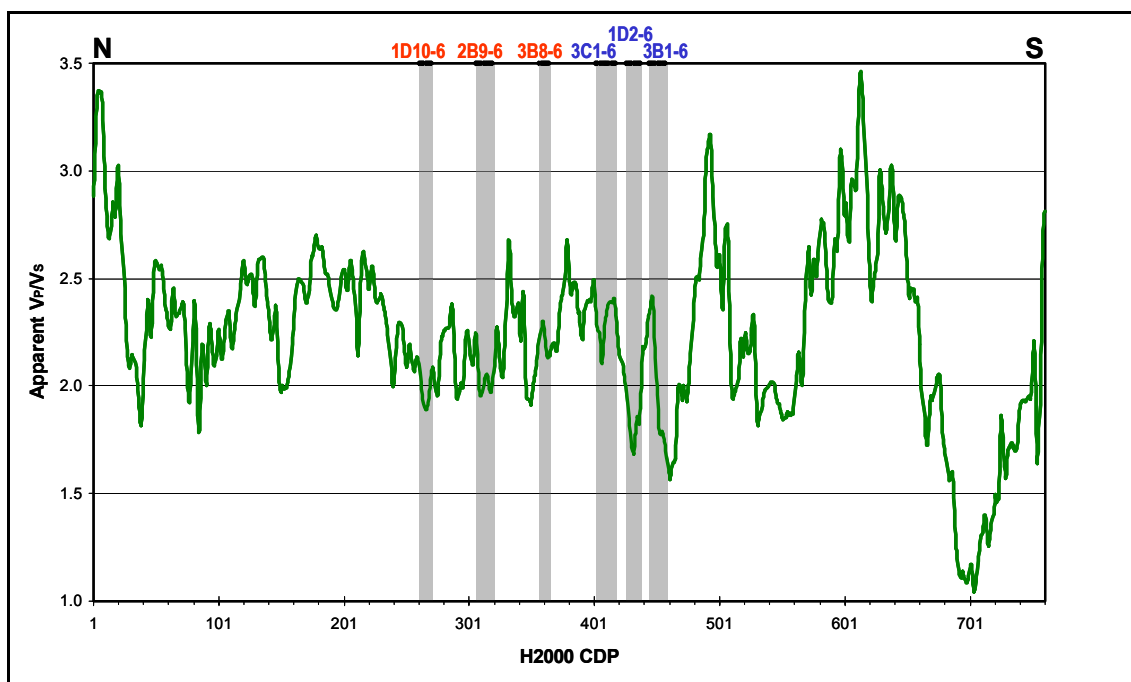


Figure 5-6:  $V_p/V_s$  plot of Waseca-Sparky interval.

Figure 5-7 is a plot of the Mannville-Lower Mannville interval. The confidence in the interpretation of this interval was much higher. The reflectors were more continuous and less impacted by noise than the Waseca-Sparky interval. Noise is still present for this interval but some distinct anomalies can be seen around the wells with the most recent steam injection. In particular the response at 3B8-6 is a pronounced drop in  $V_p/V_s$ . Steam injection was occurring in this well at the time of the 2000 seismic acquisition.

The width of the anomaly fits very well with the predicted steam zone radius. At the wells 1D10-6 and 2B9-6 there is little to no steam response. It had been 12 and 26 months, respectively, since steam had been injected in these wells. There some apparent anomalies in the CDP range 390 - 450. These are not interpreted to be real anomalies. The horizon interpretation within this CDP range on the P-S section (Figure 5-5) was very low confidence. The converted-wave data had a lower signal-to-noise ratio along this portion of the seismic line. The noise of the pumpjacks, which were in operation during the H2000 acquisition, overwhelmed the real converted-wave data signal. Some pumpjacks were only a few metres away from the geophones. The P-P section was either less contaminated with this noise (Figure 5-4), or the P-P data processing was able to remove more of it.

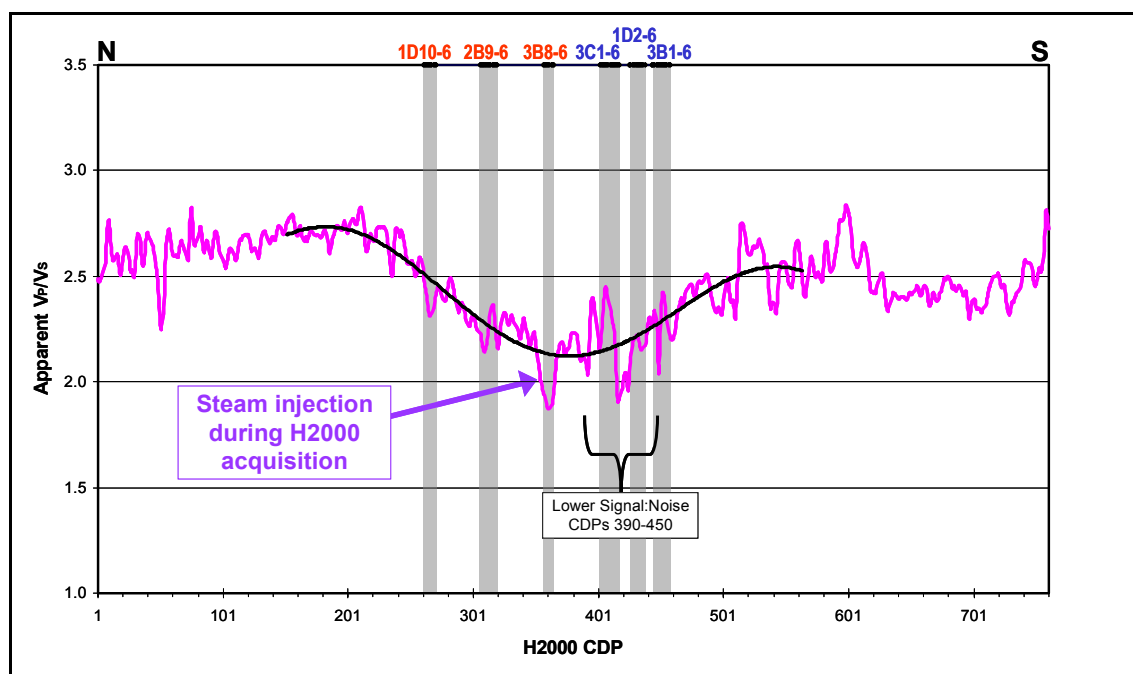


Figure 5-7:  $V_p/V_s$  plot of Mannville-Lower Mannville interval.

#### 5.4 $V_p/V_s$ Sand Percent Analysis

In addition to the anomalous drop in  $V_p/V_s$  at the 3B8-6 well, it can be qualitatively observed (Figure 5-7) that on the scale of the entire seismic line there is a smooth trend line in  $V_p/V_s$ . This long-period effect corresponds to the thickest Waseca sands in the central portion of the line. The shale content is higher in the wells to the north and south. This is similar to the lateral lithology effect that was observed at the Blackfoot oilfield (Stewart et al., 1996, Margrave et al., 1998).

The low frequency trend observed in  $V_p/V_s$  analysis (Figure 5-7) has a high correlation with an evaluation of the sand percent in the wells along the H2000 2D profile. Only a few wells penetrate to the Lower-Mannville marker used in the  $V_p/V_s$  analysis. Within the Mannville-Lower Mannville interval above and below the Waseca, it appears that there is no other significant clean sand unit (less than 3 m). Shale and silt are the main rock types directly above and below the Waseca. On the right axis of Figure 5-8 is a plot of the percent of sand in the Waseca interval. The percent sand was measured by taking the net pay (less than 45 API units on the gamma ray log) and comparing it to the gross thickness of the Waseca. For example, the gamma ray log from well 3B9-6 (Figure 5-9) has 18 m of clean sand using the 45 API units cut-off. The Waseca is 31.7 m thick at this well. Therefore, 57 percent of the Waseca is clean sand at this well location. This measurement was made for 23 (of 24) wells within 100 m of H2000. One well was excluded because it was an outlier and over 100 m east of the H2000 survey. The geology or sand percent in the reservoir can vary significantly over short distances (less than 50 m). The trends of  $V_p/V_s$  and the percent sand in the wells match very well.

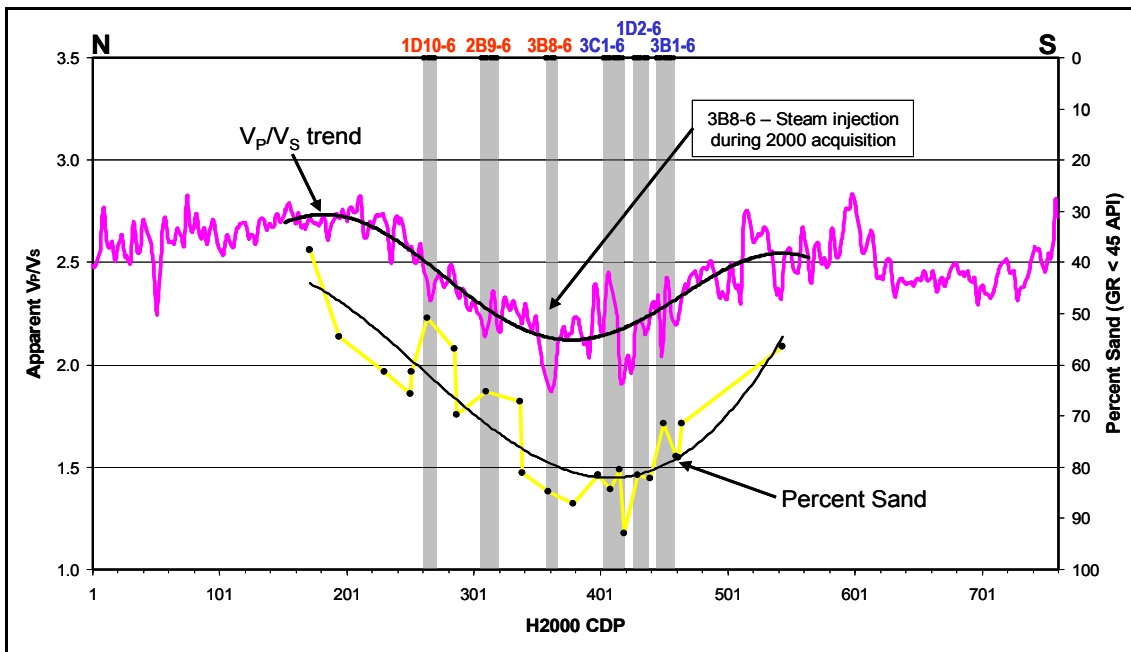


Figure 5-8: Comparison of  $V_p/V_s$  trend line (left axis) with percent sand (reversed right axis) in the wells along H2000 (converted wave).

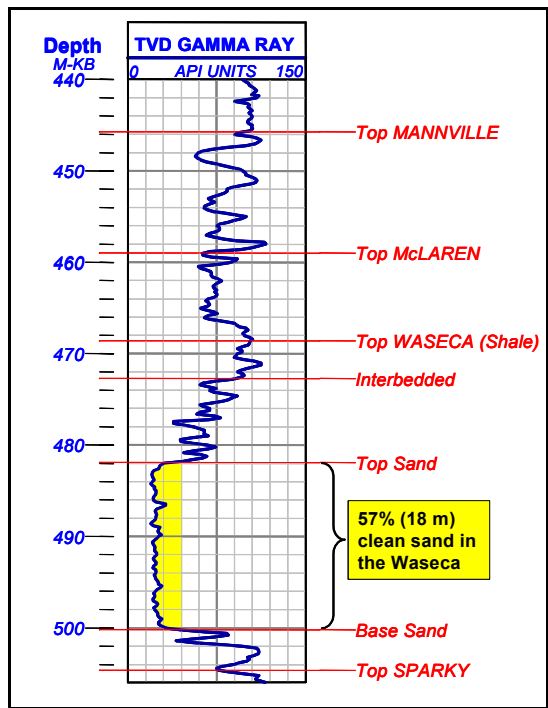


Figure 5-9: Gamma ray log from well 3B9-6 indicating 57 percent sand (or 18 m) within the Waseca interval using a 45 API units cut-off.

Figure 5-10 is a cross-plot of sand percent versus  $V_p/V_s$ , taken from the polynomial trend line. The polynomial trend line filters out the effects of steam injection and noise. This cross-plot gives a 79 percent correlation coefficient using the 23 wells. It suggests that  $V_p/V_s$  can be a robust method to discern sand quality in a mixed lithology reservoir.

The 79 percent correlation appears to be high given the quick lateral changes in geology and the noisy data. During the acquisition of the data there may have been scattered energy or offline effects that are part of the recorded signal. The processing and migration of the data reduced these effects but did not properly collapse the Fresnel zone for out of plane energy. Migration of a 2D seismic line only properly collapses the Fresnel zone in the 2D line direction (Bancroft, 1996).

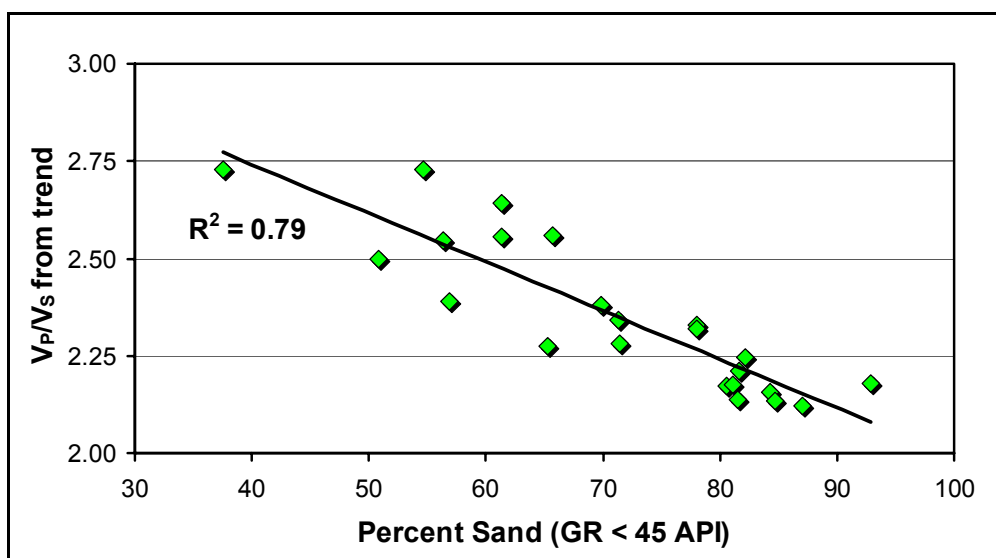


Figure 5-10: Cross plot of  $V_p/V_s$  trend line versus percent Waseca sand in 23 wells along H2000.

The Fresnel zone for unmigrated seismic data can be estimated using the Sheriff or Berkhout criterion (Lindsay, 1990). The Sheriff criterion is based on an interpretive

resolution of a quarter of a wavelet and Berkhout is based on an eighth of a wavelet. Considering the case of the P-P data with a frequency ( $f$ ) of 100 Hz, a velocity ( $V_p$ ) of 2300 m/s and a depth ( $z$ ) of 500 m, the Fresnel diameter using the Berkhout criterion can be calculated as follows:

$$F_{Berkhout} \approx \sqrt{\frac{zV_p}{f}} = \sqrt{\frac{500 * 2500}{100}} \approx 112m$$

This calculation suggests that scattered and unmigrated energy from approximately 56 m on either side of the 2D seismic lines would be contributing to the signal in the sections. Some of the offline energy would be mitigated by stacking the data because it would not stack constructively given the longer traveltimes for a given deep reflector. The stacked sections may be smeared by these offline effects. If it were available, a 3D seismic survey would be ideal to remove the offline effects because a 3D migration could be done and collapse the Fresnel zone in all directions.

## Chapter 6

### Conclusions

#### 6.1 Conclusions

The Pikes Peak field provides an excellent location to study methods to monitor heavy-oil recovery and to integrate various data types. The field has an abundance of well, seismic and engineering data, a well-defined geological story, and is a work in progress.

The time-lapse analysis of the two lines shot nine years apart is very encouraging. The reflectivity difference shows the effect of increased traveltime of the seismic signal through the reservoir zone. The impedance difference indicates lower impedance in the reservoir zone as well but not excluded to the production area. It is difficult to clearly identify and quantify differences in the sections caused by noise and changes in acquisition parameters and conditions though it is suspected that they exist. The spatial sampling of this project was restricted to one 2-D vertical section. For a more powerful analysis time-lapse 3-D seismic data is required. 3-D would not only provide better spatial sampling but a greater statistical verification of results with direct ties to well data. This process could be followed to create maps or volumes that indicate potential in-fill well locations.

With interpreted converted seismic sections, the  $V_P/V_S$  method proved to be a very powerful to observe the effective steam zone for heavy-oil reservoirs. A direct steam response can be inferred from the  $V_P/V_S$  analysis. The time-lapse isochron analysis

provided clues about the extent of the heated reservoir both in 1991 and 2000. These results, based on interval interpretations, are very sensitive to tuning and resolution. Bandwidth and phase must be carefully considered during interpretation to ensure that the same depth equivalent events are being tracked. In general, the anomalies were located where expected based on drilling results and injection/production data.

Table 6-1: Summary of seismic interpretation and analysis techniques at Pikes Peak.

<b>Analysis</b>	<b>Advantages</b>	<b>Disadvantages</b>
Reflectivity Differencing	<ul style="list-style-type: none"> <li>• Observe changes in the reservoir with time</li> </ul>	<ul style="list-style-type: none"> <li>• Requires calibration of amplitude and phase</li> <li>• Requires multiple surveys</li> </ul>
Acoustic Impedance Differencing	<ul style="list-style-type: none"> <li>• Observe changes in the reservoir with time</li> <li>• Interval property (AI) analysis</li> </ul>	<ul style="list-style-type: none"> <li>• Requires calibration of amplitude and phase</li> <li>• Requires multiple surveys</li> <li>• Reflectivity data needs to be inverted (well logs are required)</li> </ul>
Isochron Ratio	<ul style="list-style-type: none"> <li>• Observe heated reservoir zone changes with time</li> </ul>	<ul style="list-style-type: none"> <li>• Tuning effects</li> <li>• Requires multiple surveys</li> </ul>
$V_p/V_s$	<ul style="list-style-type: none"> <li>• Observe steam front</li> <li>• Observe lateral lithology changes</li> <li>• Only one survey required</li> <li>• Acquire 3-C data</li> </ul>	<ul style="list-style-type: none"> <li>• Resolution of P-S data</li> <li>• Geophones need to be oriented; higher cost</li> <li>• Cannot observe changes with time (unless time-lapse multicomponent surveys are acquired)</li> </ul>

All four methods of detecting steam fronts show general consistency in detecting the steam and heated zones. Three of these methods indicate that differencing in surveys for reflectivity impedance, and P-wave traveltimes indicate steam zones. This application of the  $V_p/V_s$  method for steam detection is new and previously unpublished. It requires multicomponent data but may be a useful detector without the use of a base or repeat surveys. Table 6-1 summarizes the advantages and disadvantages of the four methods.

Trace-based inversion makes use of a priori knowledge to constrain results. In this case study acoustic impedance logs and horizon interpretations guided the inversion process. The low end of the spectrum from the earth model was merged with the band-limited inverted result to optimize the spectrum content. Acoustic impedance data is an interval property that can be directly related to rock properties. In this case study a decrease in impedance in the Waseca interval was found as expected. Inversion is an inexpensive analysis tool that enhances the understanding of reflectivity data.

Seismic data have the advantage of imaging a larger and continuous portion of the subsurface than well data can provide. The cost is resolution. Working within the boundaries of that resolution and appropriate scaling of well data allow the integration of the two data types. The geological interpretation and understanding of a complex structural and stratigraphic reservoir can be greatly enhanced through well-to-seismic data integration. The salt isochron analysis provides a predictive tool to assess the risk of encountering bottom water in the Waseca reservoir at Pikes Peak. The  $V_p/V_s$  method can predict with high confidence where the thickest clean sands are found. Both of these

methods can be used as the geoscientists and engineers delineate the remaining potential in the Waseca reservoir at Pikes Peak.

The results of the  $V_p/V_s$  analysis, both for steam front delineation and lithology prediction, show how much reservoir surveillance and understanding can be gathered from a single multicomponent survey at any time in the development of a field.

## 6.2 Future Research

Listed in Chapter 1.2 are many papers, posters and theses that have already been published using the Pikes Peak data. Topics previously investigated have included: seismic attenuation, anisotropy, vibroseis deconvolution, AVO (Amplitude Versus Offset), joint inversion, reservoir simulation, VSP acquisition and processing, 3-C lake-bottom data acquisition, and noise suppression. This list is impressive but there are a number of investigations that may be considered by future researchers with this Pikes Peak or similar data sets.

1. Work could be done to evaluate the seismic sections in depth rather than time. Velocity models for the time-lapse data would include the velocity perturbations required to observe the time lag associated with the reflectivity difference section (Figure 4-3). Comparisons of H1991 and H2000 velocities models could be made to further understand the anomalies seen in the time data. All of the data in depth may allow more detailed correlations of geological, petrophysical and engineering data.

2. Geostatistical methods could be applied to further integrate the well logs with seismic reflectivity or impedance data. The prediction of reservoir properties such as fluid saturations (bottom water) and porosity distribution in the Waseca interval may be possible. A more detailed interpretation of the three facies units within the Waseca interval could be another potential outcome. Geostatistical software modules are available in Hampson-Russell and Jason.
3. The interpretation of the P-P and P-S sections from the multicomponent survey could be done in relatively new software, Hampson-Russell ProMC. The interpretations would be more tightly constrained and a  $V_p/V_s$  model would result that may further explain and quantify some of the steam and lithology anomalies.
4. The analysis and integration of the 3-C VSP and lake-bottom data could provide additional insights and constraints on the results of this thesis.

There is a risk of over-interpreting this 2-D seismic data given the resolution of the data and the necessity to project well data onto to a single line of section. The condition of reservoir is continually changing as the resource is depleted and more wells are drilled for steam injection and production. Future research is strongly encouraged but these limitations and the dynamic nature of the reservoir must be carefully considered.

## References

- Bancroft, J.C., 1996, A practical understanding of pre- and poststack migration: Society of Exploration Geophysics, Tulsa, OK.
- Bates, R.L. and Jackson, J.A., 1984, Ed., Dictionary of geological terms: 3rd ed., American Geological Institute.
- Buxton Latimer, R., Davison, R., and Van Riel, P., 2000, An interpreter's guide to understanding and working with seismic-derived acoustic impedance data: *The Leading Edge*, **19** (3), 242-256.
- Brittle, K. F., Lines, L. R. and Dey, A. K., 2001, Vibroseis deconvolution: a comparison of cross-correlation and frequency-domain sweep deconvolution: *Geophys. Prosp., Eur. Assn. Geosci. Eng.*, **49**, 675-686.
- Chen, S., Lines, L.R., Embleton, J., Daley, P.F., and Mayo, L., 2003, Seismic detection of wormholes in heavy oil: 2003 CSEG Annual Mtg, Calgary, Alberta, 2-6 June.
- de Buyl, M., 1989, Optimum field development with seismic reflection data: *The Leading Edge*, **8** (4), 14-20.
- Dey, A.K., Stewart, R.R, Lines, L.R., and Bland, H.C., 2000, Noise suppression on geophone data using microphone measurements: Univ. of Calgary CREWES Research Report, **12**, 81-92.
- Downton, J.E. and Lines, L.R., 2000, Preliminary results of the AVO analysis at Pike's Peak: Univ. of Calgary CREWES Research Report, **12**, 523-531.
- Eastwood, J., 1993, Temperature – dependent propagation of P- and S-waves in Cold Lake oil sands: Comparison of theory and experiment: *Geophysics*, **58**, 863-872.
- Eastwood, J., Lebel, P., Dilay, A., and Blakeslee, S., 1994, Seismic monitoring of steam-based recovery of bitumen: *The Leading Edge*, **13** (4), 242-251.
- Hedlin, K., Mewhort, L. and Margrave, G., 2001, Delineation of steam flood using seismic attenuation: 71st Ann. Internat. Mtg: Soc. of Expl. Geophys., 1572-1575.
- Hoffe, B.H., Bertram, M.B., Bland, H.C., Gallant, E.V., Lines, L.R., and Mewhort, L.E., 2000, Acquisition and processing of the Pikes Peak 3-C 2-D seismic survey: Univ. of Calgary CREWES Research Report, **12**, 511-522.
- Husky Energy Inc, 2001, Husky Lloydminster Upgrader – Upgrader, corporate brochure.

- Isaac, J.H., 1996, Seismic methods for heavy oil reservoir monitoring: Ph. D. thesis, Univ. of Calgary, Dept. of Geology and Geophysics.
- Justice, J. H., 1992, Geophysical methods for reservoir surveillance, *in* Sheriff, R. E., Ed., Reservoir geophysics: Soc. of Expl. Geophys., 281-284.
- Lindseth, R., 1979, Synthetic sonic logs – a process for stratigraphic interpretation: Geophysics, **44**, 3-26.
- Lindsey, J. P., 1990, The Fresnel zone and its interpretive significance, *in* Lynch, K. J., Ed., Seismic interpretation series: Soc. of Expl. Geophys., 37-43.
- Lines, L.R., Jackson, R., and Covey, J.D., 1990, Seismic velocity models for heat zones in Athabasca tar sands: Geophysics, **55**, 1108-1111.
- Margrave, G.F., Lawton, D.C., and Stewart, R.R., 1998, Interpreting channel sands with 3C-3D seismic data: The Leading Edge, **17** ( 4), 509-513.
- Matthews, L., 1992, 3-D seismic monitoring of an in-situ thermal process: Athabasca Canada: *in* Sheriff, R., Ed., Reservoir Geophysics, Soc. Expl. Geophysics, 301-308.
- McQuillin, R., Bacon, M., and Barclay, W., 1984, An introduction to seismic interpretation: Gulf Publishing Company, Houston.
- Meyer, R.F., and De Witt Jr., W., 1990, Definition and world resources of natural bitumens: U.S. Geological Survey Bulletin 1944, 1-14.
- Miller, S.L.M., (1996), Multicomponent seismic data interpretation: M.Sc. thesis, Univ. of Calgary, Dept. of Geology and Geophysics.
- Newrick, R., Lawton, D., and Spratt, D., 2001, Seismic velocity anisotropy analysis at Pike's Peak, Saskatchewan, Canada: 71st Ann. Internat. Mtg: Soc. of Expl. Geophys., 98-101.
- Nur, A. and Wang, Z., 1989, Ed., Seismic and acoustic velocities in reservoir rocks, 1 - experimental studies: Soc. of Expl. Geophys., 1-6.
- Nur, A., 1982, Seismic imaging in enhanced recovery: SPE/DOE 3rd Ann. Joint symposium on enhanced oil recovery, 99-109.
- Osborne C.A. and Stewart, R.R., 2001, Analyzing the Pikes Peak multi-offset VSP data set: Univ. of Calgary CREWES Research Report, **13**, 763-776.

- Pullin, N., Matthews, L., and Hirshe, K., 1987b, Techniques applied to obtain very high resolution 3-D seismic imaging at an Athabasca tar sands thermal plot: *The Leading Edge*, **6** (12), 10-15.
- Richardson, J. G. and Sneider, R. M., 1992, Synergism in reservoir management, *in* Sheriff, R. E., Ed., *Reservoir geophysics: Soc. of Expl. Geophys.*, 6-11.
- Schmitt, D.R., 1999, Seismic attributes for monitoring of a shallow heated heavy oil reservoir: A case study: *Geophysics*, **64** (2), 368-377.
- Sheppard, G.L., Wong F.Y.F., and Love D., 1998, Husky's success at the Pikes Peak thermal project: UNITAR International Conference on Heavy Crude and Tar Sands, Beijing, China.
- Sheriff, R. E., 1991, Encyclopedic dictionary of exploration geophysics: *Soc. of Expl. Geophys.*, 384.
- Sheriff, R. E., 1992, Basic petrophysics and geophysics, *in* Sheriff, R. E., Ed., *Reservoir geophysics: Soc. of Expl. Geophys.*, 37-49.
- Stewart, R.R., Ferguson, R., Miller, S., Gallant, E., and Margrave, G., 1996, The Blackfoot seismic experiments: broad-band, 3C-3D and 3-D VSP surveys: *CSEG Recorder*, **21** (6), 7-10.
- Stewart, R. R., Bland, H. C., Zhang, O. and Guthoff, F., 1997, Average versus interval  $V_P/V_S$ : *J. Can. Soc. Expl. Geophys.*, **33** (1 & 2), 29-31.
- Stewart, R.R., Lines, L.R. and Mewhort, L.E., 2000, Multicomponent VSP and lake-bottom cable surveys – Pikes Peak, Saskatchewan: Univ. of Calgary CREWES Research Report, **12**, 35-42.
- Sun, Z, 1999, Seismic Methods for Heavy Oil Reservoir Monitoring and Characterization: Ph. D. thesis, Univ. of Calgary, Dept. of Geology and Geophysics.
- Van Hulten, F.F.N., 1984, Petroleum geology of Pikes Peak heavy oil field, Waseca Formation, Lower Cretaceous, Saskatchewan: Canadian Society of Petroleum Geologists, Memoir 9, 441-454.
- Wang, Z. and Nur, A., 1988, Effect of temperature on wave velocities in sands and sandstones with heavy hydrocarbons: *SPE Res. Eng.*, **3**, 158-164.
- Wang, Z. and Nur, A., 1992, Aspects of rock physics in seismic reservoir surveillance, *in* Sheriff, R. E., Ed., *Reservoir geophysics: Soc. of Expl. Geophys.*, 285-300.

- Watson, I.A., Brittle, K.F., and Lines, L.R., 2001, Reservoir characterization using elastic wave properties: Univ. of Calgary CREWES Research Report, **13**, 777-784.
- Watson, I.A. and Lines, L.R., 2000, Seismic inversion at Pikes Peak, Saskatchewan: Univ. of Calgary CREWES Research Report, **12**, 533-538.
- Watson, I.A. and Lines, L.R., 2001, Time-lapse seismic monitoring at Pikes Peak, Saskatchewan: 2001 CSEG Annual Mtg, Calgary, Alberta, 29 April – 4 May. .
- Watson, I.A. and Lines, L.R., 2003, Geological interpretations from seismic data at Pikes Peak, Saskatchewan: Univ. of Calgary CREWES Research Report, **15**.
- Watson, I.A., Lines, L.R., and Brittle, K.F., 2002, Heavy-oil reservoir characterization using elastic wave properties, *The Leading Edge*, **21** (8), 736-739.
- Wong, F.Y.F., Anderson, D.B., O'Rourke, J.C., Rea, H.Q. and Scheidt, K.A., 2001, Meeting the challenge to extend success at the Pikes Peak steam project to areas with bottom water: 2001 SPE Annual Technical Conference and Exhibition, New Orleans, 30 September - 3 October.
- Xu, C., 2001, Processing the Pikes Peak walkaway VSP survey and estimating a Q-factor: AOSTRA Project 1296.
- Zhang, H., 2003, Interpretive PP and PS Joint Inversion: M.Sc. thesis, Univ. of Calgary, Dept. of Geology and Geophysics.
- Zou, Y., Bentley, L.R., and Lines, L.R., 2002, Time-lapse seismic modelling of the Pikes Peak field: Univ. of Calgary CREWES Research Report, **14**.
- Zou, Y., Bentley, L.R., and Lines, L.R., 2003, Integration of reservoir simulation with time-lapse seismic modelling: Univ. of Calgary CREWES Research Report, **15**.

## Appendix A General Well Data

Table A-1: Summary of 24 Pikes Peak wells adjacent to H1991 and H2000 seismic lines.

	UWI	Short ID	Rig Release Date	KB (m ASL)	TD (m)	TVD (m)	Surface Location X (UTM)	Surface Location Y (UTM)	Bottom Hole Location X (UTM)	Bottom Hole Location Y (UTM)	Deviation X (m)	Deviation Y (m)	Distance from H2000 (m)	CURVES*
1	111153104923W300	A15-31	Dec-78	612.3	587.0	587.0	609877.7	5903926.6	609863.5	5904321.4	27.9	-74.3	-92.3	A
2	114020605023W300	5A2-6	Mar-98	619.9	557.0	548.3	609835.6	5904395.7	609863.5	5904321.4	27.9	-74.3	-97.1	A
3	112020605023W300	1A2-6	Nov-85	620.6	618.9	521.5	609865.7	5904504.0	609905.1	5904338.2	239.4	-165.8	-55.1	A
4	111020605023W300	A2-6	Oct-78	618.1	588.9		609868.0	5904349.3	609905.1	5904338.2			-92.0	A
5	121010605023W300	3B1-6	Jan-82	615.4	515.1		610017.7	5904402.5	609905.1	5904338.2			58.9	A
6	150020605023W300	4A2-6	Dec-82	617.5	520.0		609865.7	5904449.4	609905.1	5904338.2			-91.9	A
7	143020605023W300	1D2-6	Nov-83	614.2	517.0		609957.3	5904498.2	609905.1	5904338.2			0.9	A
8	141020605023W300	D2-6	Feb-81	616.3	516.0		609863.0	5904549.7	609905.1	5904338.2			-92.1	B
9	142020605023W300	10BS2-6	May-81	616.3	520.0		609863.0	5904565.1	609905.1	5904338.2			-91.7	A
10	131010605023W300	3C1-6	Nov-83	613.5	515.7		609982.1	5904606.8	609905.1	5904338.2			28.2	A
11	181020605023W300	4D2-6	Dec-82	615.1	516.9		609861.0	5904650.7	609905.1	5904338.2			-91.7	A
12	111070605023W300	A7-6	Jan-79	615.7	591.6		609846.8	5904749.4	609905.1	5904338.2			-103.5	A
13	193080605023W300	3B8-6	Feb-95	617.0	601.0	537.0	609835.8	5904718.0	609982.3	5904853.1	146.5	135.1	34.3	A
14	131080605023W300	3C8-6	Jun-99	604.4	525.0	516.4	610003.3	5904956.6	610056.1	5904968.4	52.8	11.8	110.9	B
15	195070605023W300	4D7-6	Jun-99	607.3	622.0	521.6	609642.6	5905088.4	609903.5	5904951.7	280.9	-136.7	-42.0	A
16	192090605023W300	2B9-6	Aug-96	603.2	566.0	533.4	609921.5	5904954.7	609973.7	5905095.6	52.2	140.9	31.6	A
17	111100605023W300	4A10-6	Jun-99	607.3	638.0	522.3	609632.2	5905095.4	609910.1	5905206.9	277.9	111.5	-29.3	A
18	195090605023W300	3B9-6	Jun-99	604.8	600.0	521.8	609991.6	5904956.3	610026.5	5905221.4	34.9	265.1	87.4	A
19	194100605023W300	1D10-6	Feb-97	605.3	664.5	529.3	609956.3	5904965.7	609918.7	5905327.5	-37.6	361.8	-17.8	A
20	141100605023W300	4D10-6	Feb-00	603.8	617.0	523.3	609594.4	5905435.4	609851.5	5905386.0	257.1	-49.4	-83.6	A
21	196090605023W300	3C9-6	Feb-00	603.8	700.0	522.3	609594.3	5905441.4	610011.0	5905397.6	416.7	-43.8	76.1	A
22	191150605023W300	1A15-6	Feb-00	603.9	642.0	524.1	609594.1	5905447.3	609926.5	5905492.1	332.4	44.8	-6.0	C
23	141150605023W300A	D15-6	Oct-78	604.1	583.1		609868.8	5905673.7	609926.5	5905492.1			-59.4	D
24	142150605023W300	4D15-06	Oct-02	609.2	596.0		609925.5	5905788.7	609926.5	5905492.1			0.0	n/a

\*CURVES

- A - Gamma Ray, Resistivity, Spontaneous Potential, Caliper, Bulk Density, Neutron Porosity
- B - Gamma Ray, Resistivity, Spontaneous Potential, Caliper, Bulk Density, Neutron Porosity, Sonic
- C - Gamma Ray, Resistivity, Spontaneous Potential, Caliper, Bulk Density, Neutron Porosity, Dipole Sonic
- D - Gamma Ray, Resistivity, Spontaneous Potential, Caliper, Sonic

## Appendix B

### Matrix Seismic Processing Flows

#### H1991

**Reformat:** Record length 2000 ms; Sample rate 2 ms

**Geometry Assignment; Trace Kills and Edits**

**Polarity Reversal:** First-break Peaks reversed to troughs

**Amplitude Recovery:** Spherical divergence correction + 4 dB/second

**Surface-Consistent Deconvolution:** Spiking

Resolved: Source, Receiver, CDP, Offset    Applied: Source, Receiver, CDP

Operator length: 60 ms; Prewhitening: 0.1%

Design window: 196-1348 ms at 0 m offset; 880-1422 ms at 1319 m offset

**Phase Compensation:** Correction for vibroseis deconvolution

**Time-Variant Spectral Whitening:** 2/8-110/130 Hz

**Refraction Statics:** Datum elevation: 630 m; Replacement velocity: 2000 m/s

**Velocity Analysis**

**Surface-Consistent Statics:** Max shift 20 ms; 4 event-tracking windows

**Normal Moveout Correction**

**Front-End Muting:** Offset (m) 180 220 600 1320 T(ms) 0 177 658 891

**Time-Variant Scaling:** Center-to-center 0-300,200-900,700-1300

**CDP Trim Statics:** Max shift 8 ms    Correlation window: 100-1200 ms

**CDP Stack:** Alpha-trimmed; reject 15%; 100 ms bulk shift

**Time-Variant Spectral Whitening:** 2/8-110/130 Hz

**Trace Equalization:** mean window 100-1200 ms

**F-X Prediction Filtering:** 40 traces by 100 ms; 50% overlap; 7 point filter

**Wave Equation Datuming:** Final Datum: -10 ms; Replacement velocity: 2000 m/s

**Migration:** Phase-shift; Aperture: 0-90 degrees; 100% smoothed stacking velocities

**Bandpass Filter:** Ormsby 10/14-110/130

**Trace Equalization:** 100-1200 ms

## **H2000 Geophone Array**

**Reformat:** Record length 16000 ms, Sample rate 2 ms

**Sum and Correlate Field Records; Extract Array Component**

**Geometry Assignment; Trace Kills and Edits**

**Amplitude Recovery:** Spherical divergence correction + 4 dB/second

**Surface-Consistent Deconvolution:** Spiking

Resolved: Source, Receiver, CDP, Offset Applied: Source, Receiver, CDP

Operator length: 60 ms; Prewhitening: 0.1%

Design window: 196-1348 ms at 0 m offset; 880-1422 ms at 1319 m offset

**Phase Compensation:** Correction for vibroseis deconvolution

**Time-Variant Spectral Whitening:** 2/8-150/170 Hz

**Refraction Statics:** Datum elevation: 630 m; Replacement velocity: 2000 m/s

**Velocity Analysis**

**Surface-Consistent Statics:** Max shift 20 ms; 4 event-tracking windows

**Normal Moveout Correction**

**Front-End Muting:** Offset (m) 180 220 600 1320 T(ms) 0 177 658 891

**Time-Variant Scaling:** Center-to-center 0-300,200-900,700-1300

**CDP Trim Statics:** Max shift 8 ms; Correlation window: 100-1200 ms

**CDP Stack:** Alpha-trimmed; reject 15%; 100 ms bulk shift

**Time-Variant Spectral Whitening:** 2/8-150/170 Hz

**Trace Equalization:** mean window 100-1200 ms

**F-X Prediction Filtering:** 40 traces by 100 ms, 50% overlap, 7 point filter

**Wave Equation Datuming:** Final Datum: -10 ms; Replacement velocity: 2000 m/s

**Migration:** Phase-shift; Aperture 0-90 degrees; 100% smoothed stacking velocities

**Bandpass Filter:** Ormsby 10/14-150/170 Hz

**Trace Equalization:** 100-1200 ms

## **H2000 Vertical Component**

**Reformat:** Record length 16000 ms, Sample rate 2 ms

**Sum and Correlate Field Records; Extract Vertical Component**

**Geometry Assignment; Trace Kills and Edits**

**Amplitude Recovery:** Spherical divergence correction + 4 dB/second

**Surface-Consistent Deconvolution:** Spiking

Resolved: Source, Receiver, CDP, Offset    Applied: Source, Receiver, CDP

Operator length: 60 ms; Prewhitening 0.1 %

Design window: 196-1348 ms at 0 m offset; 880-1422 ms at 1319 m offset

**Phase Compensation:** Correction for vibroseis deconvolution

**Time-Variant Spectral Whitening:** 2/8-150/170 Hz

**Refraction Statics:** Datum elevation 630 m Replacement velocity 2000 m/s

**Velocity Analysis**

**Surface-Consistent Statics:** Max shift 20 ms 4 event-tracking windows

**Normal Moveout Correction**

**Front-End Muting:** Offset (m) 180 220 600 1320; T(ms) 0 177 658 891

**Time-Variant Scaling:** Center-to-center: 0-300, 200-900, 700-1300

**CDP Trim Statics:** Max shift 8 ms; Correlation window: 100-1200 ms

**CDP Stack:** Alpha-trimmed; reject 15%; 100 ms bulk shift

**Time-Variant Spectral Whitening:** 2/8-150/170 Hz

**Trace Equalization:** mean window 100-1200 ms

**F-X Prediction Filtering:** 40 traces by 100 ms; 50% overlap; 7 point filter

**Wave Equation Datuming:** Final Datum: -10 ms; Replacement velocity: 2000 m/s

**Migration:** Phase-shift; Aperture 0-90 degrees; 100% smoothed stacking velocities

**Bandpass Filter:** Ormsby 10/14-150/170 Hz

**Trace Equalization:** 100-1200 ms

## H2000 Radial Component

**Reformat:** Record length 16000 ms, Sample rate 2 ms

**Sum & Correlate Field Data; Extract Horizontal Components; Rotate Into Slow Assign Geometry; Asymptotic Binning** ( $V_P/V_S = 3.16$ )

**Reverse Polarity of Negative Offsets; Trace Kills & Edits**

**Amplitude Recovery:** Spherical divergence correction + 4 dB/second

**Shot f-k Filter:** Arbitrary polygons to remove source noise

**Surface-Consistent Deconvolution:** Spiking

Resolved: Source, Receiver, CDP, Offset    Applied: Source, Receiver, CDP

Operator length: 90 ms; Prewhitening: 0.1%

Design window: 252-2453 ms at 10 m offset; 1156-2529 ms at 1319 m offset

**Phase Compensation:** Correction for vibroseis deconvolution

**Time-Variant Spectral Whitening:** 2/8-60/80 Hz

**Structure Statics:** source from vertical data, receiver from shear refraction

**Velocity Analysis**

**Residual Receiver Statics**

**Surface-Consistent Statics:** Max shift 20 ms; 3 event-tracking windows

**Converted-Wave NMO Correction**

**Front-End Muting:** Offset (m) 210 250 640 960 1310; T (ms) 0 410 810 1256 1500

**Time-Variant Scaling:** Center-to-center 0-600,400-1700, 1400-2400, 2100-3400

**ACP Trim Statics:** Max shift 12 ms; Correlation window: 350-2350 ms

**Converted-Wave Stack:**  $V_P/V_S$  from vertical correlations; +300 ms bulk shift

**Time-Variant Spectral Whitening:** 2/8-60/80 Hz

**Trace Equalization:** mean window 200-1900 ms

**F-X Prediction Filtering:** 40 traces by 150 ms; 50% overlap; 7 point filter

**Migration:** Kirchhoff; Aperture 0-40 degrees; 100% P-S migration velocities

**Bandpass Filter:** Ormsby 2/8-40/50 Hz

**Trace Equalization:** 200-1900 ms

## Appendix C

### Engineering Well Data

Table C-1: Husky engineering data as of February 15, 1991.

Well	Rig Release Date	Well Status	Predicted Steam Radius (m)	Reservoir Pressure <sup>2</sup> (kPa)	Temperature <sup>3</sup> (°C)	Cum. Oil m <sup>3</sup>	Cum. Water m <sup>3</sup>	Cum. Steam m <sup>3</sup>
A15-31	Dec-78	abandoned		virgin				
5A2-6	Mar-98	not drilled		virgin				
1A2-6	Nov-85	suspended - last produced 10-Oct-1988	20.2	3100 (Mar-93)	50.0	12738.5	27711.1	25015.1
A2-6	Oct-78	not perforated in Waseca		virgin				
3B1-6	Jan-82	producer	6.0	2900 (Jan-91)		817.5	7146.3	16531.0
4A2-6	Dec-82	suspended - last produced 17-Jun-1986	25.5	3400 (Nov-92)	80.0	20472.0	25100.9	57584.4
1D2-6	Nov-83	suspended - last produced 23-Dec-1986	22.3	2900 (Sep-92)	60.0	14101.9	49832.6	23285.0
D2-6	Feb-81	suspended - last produced 14-Apr-1987	25.4	2300 (Sep-92)	50.0	20847.7	46054.5	30341.0
10BS2-6	May-81	observation						
3C1-6	Nov-83	suspended - last produced 27-May-1986	19.8	3400 (Mar-92)	64.0	11321.5	42346.0	13853.9
4D2-6	Dec-82	suspended - last produced 8-Feb-1986	21.6	2900 (Sep-93)	100.0	14699.0	52225.2	33463.3
A7-6	Jan-79	not drilled		virgin				
3B8-6	Nov-95	not drilled		virgin				
3C8-6 <sup>4</sup>	Jun-99	n/a		n/a				
4D7-6	Jun-99	not drilled		virgin				
2B9-6	Aug-96	not drilled		virgin				
4A10-6	Jun-99	not drilled		virgin				
3B9-6	Jun-99	not drilled		virgin				
1D10-6	Feb-97	not drilled		virgin				
4D10-6	Feb-00	not drilled		virgin				
3C9-6	Feb-00	not drilled		virgin				
1A15-6	Feb-00	not drilled		virgin				
D15-6	Oct-78	no perforations		virgin				
4D15-06	Oct-02	not drilled		virgin				
<b>Total</b>						<b>94998.0</b>	<b>250416.5</b>	<b>200073.7</b>

**Notes:**

- 1 - Data provided by Husky Energy (see Chapter 1.4.3)
- 2 - Estimate from casing injection pressure; closest data available to February 1991. Virgin pressure is estimated to be 2200 kPa.
- 3 - Estimate from production tubing temperature
- 4 - 3C8-6 was included because it has sonic and density logs. Husky did not provide data for this well.

Table C-2: Husky engineering data as of March 1, 2000.

Well	Rig Release Date	Well Status	Predicted Steam Radius <sup>1</sup> (m)	Reservoir Pressure <sup>2</sup> (kPa)	Temperature <sup>3</sup> (°C)	Cum. Oil m <sup>3</sup>	Cum. Water m <sup>3</sup>	Cum. Steam m <sup>3</sup>
A15-31	Dec-78	abandoned	11.0	2900 (Sep-93)	62.0	3072.36	5802.48	5995.93
5A2-6	Mar-98	producer	20.2	3100 (Mar-93)	135.0	35149.2	116897.3	37081.9
1A2-6	Nov-85	suspended - last produced 22-Feb-1997	26.7	1200 (Jul-99)	108.0	19216.6	28911.2	39246.6
A2-6	Oct-78	producer	44.1	1200 (Nov-99)	111.0	44062.2	227634.0	64433.0
3B1-6	Jan-82	producer	30.8	3400 (Nov-92)	104.0	30033.5	94785.4	63673.7
4A2-6	Dec-82	producer	31.5	1800 (Jan-98)	148.0	27961.5	124356.7	52865.8
1D2-6	Nov-83	producer	25.4	1300.0	190.0	20847.7	46054.5	408506.4
D2-6	Feb-81	injector						
10BS2-6	May-81	observation						
3C1-6	Nov-83	producer	44.2	3400 (Mar-92)	123.0	56414.9	237328.5	25751.0
4D2-6	Dec-82	producer	29.4	2900 (Sep-93)	58.0	27158.7	181498.6	42227.0
A7-6	Jan-79	no Wassaca perforations	n/a	n/a	n/a	n/a	n/a	n/a
3B8-6	Feb-95	injector	25.4	1400.0	190.0	22206.3	20056.24	190106.45
3C8-6 <sup>4</sup>	Jun-99	n/a		n/a	n/a			
4D7-6	Jun-99	producer	8.0	3000 (Feb-00)	90.0	1987.07	842.33	7673.94
2B9-6	Aug-96	producer	37.2	2400 (Apr-00)	82.0	35697.42	26295.43	26978.18
4A10-6	Jun-99	producer	10.4	4000 (Feb-00)	113.0	2747.24	1483.66	7810.18
3B9-6	Jun-99	producer	11.2	4000 (Mar-00)	88.0	2380.86	629.32	7901.31
1D10-6	Feb-97	producer	29.8	3000 (May-00)	90.0	18737.83	39233.26	33029.28
4D10-6	Feb-00	not drilled		virgin				
3C9-6	Feb-00	not drilled		virgin				
1A15-6	Feb-00	not drilled		virgin				
D15-6	Oct-78	no perforations		virgin				
4D15-06	Oct-02	not drilled		virgin				
Total						347673.3	1151808.8	1013280.6

## Notes:

- 1 - Data provided by Husky Energy (see Chapter 1.4.3)
- 2 - Estimate from casing injection pressure; closest data available to March 2000. Virgin pressure is estimated to be 2200 kPa.
- 3 - Estimate from production tubing temperature
- 4 - 3C8-6 was included because it has sonic and density logs. Husky did not provide data for this well.